

Signal-Multiplexing Ranging for Network Localization

Zijian Zhang[✉], *Student Member, IEEE*, Hanying Zhao[✉], *Student Member, IEEE*,
Jian Wang[✉], *Senior Member, IEEE*, and Yuan Shen[✉], *Senior Member, IEEE*

Abstract—Precise range information is essential for high-precision network localization, where clock drifts will severely degrade the ranging accuracy. Two-way ranging methods are commonly adopted to mitigate those effects in localization networks but requiring a large amount of signal transmission to measure the distance between all pairs of nodes. This paper establishes a network localization framework, which fully mitigates clock drifts using only a minimum number of signal transmissions. The enabler is the proposed signal-multiplexing network ranging (SM-NR) method that minimizes communication overhead via signal multiplexing and eliminates clock drifts by exploiting the interconnections of timestamps. The proposed localization framework also allows some nodes to work in silent mode, of which the positions can be precisely determined without extra ranging signal transmissions. Simulation results show that the proposed algorithm can achieve high-precision localization in the presence of clock drifts with minimum signal overhead.

Index Terms—Network ranging, localization, clock drift, time of flight, time difference of flight.

I. INTRODUCTION

REAL-TIME high-precision localization service plays a vital role in multifarious emerging applications such as the Internet-of-Things (IoT) and autonomous vehicles. The global positioning system (GPS) is the most common localization infrastructure, while its effectiveness is limited in harsh propagation environments, e.g., buildings, subways, and mines [1]–[3]. Network localization owns the merits of low-cost and wide-coverage and has the potential to achieve sub-meter level localization accuracy in GPS-challenged scenarios [4]–[6].

Manuscript received December 18, 2020; revised June 20, 2021; accepted August 9, 2021. Date of publication August 26, 2021; date of current version March 10, 2022. This work was supported in part by the Basic Research Strengthening Program of China (173 Program) under Grant 2020-JCJQ-ZD-015-01, in part by the National Key Research and Development Program of China under Grant 2020YFC1511803, and in part by the National Natural Science Foundation of China under Grant 61871256. The associate editor coordinating the review of this article and approving it for publication was W. Ni. (Zijian Zhang and Hanying Zhao contributed equally to this work.) (Corresponding author: Yuan Shen.)

The authors are with the Department of Electronic Engineering, Tsinghua University, Beijing 100084, China, and also with Beijing National Research Center for Information Science and Technology, Tsinghua University, Beijing 100084, China (e-mail: zhangzj20@mails.tsinghua.edu.cn; zhao-hy16@mails.tsinghua.edu.cn; jian-wang@tsinghua.edu.cn; shenyuan_ee@tsinghua.edu.cn).

Color versions of one or more figures in this article are available at <https://doi.org/10.1109/TWC.2021.3106172>.

Digital Object Identifier 10.1109/TWC.2021.3106172

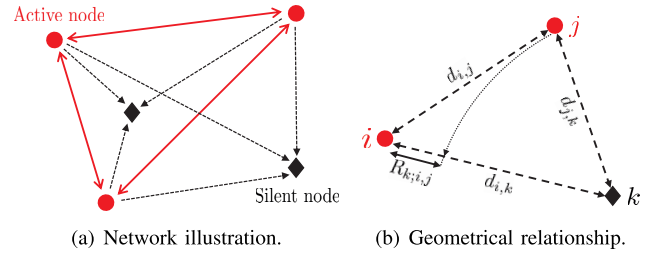


Fig. 1. (a) An illustration of an asynchronous network with three active nodes and two silent nodes. (b) The geometrical relationship between the absolute range $d_{i,j}$ and the differential range $R_{k;i,j}$, where i, j are two active nodes and k is a silent node.

Precise range information is desired in network localization systems to achieve high-precision results, which is commonly obtained by measuring wideband signal propagation time thanks to its high temporal resolution [7]–[9]. However, due to inherent clock characteristics such as the deviations of the electronic components from their nominal values, and external factors, such as voltage changing and hardware aging, there exists a significant frequency deviation between the true time and the clock time [10]–[13], which will greatly influence the ranging performance. For example, for a commercial crystal-quartz clock oscillator with frequency varying up to 40 ppm, the clocks will loose 40 ns in a millisecond and result in range error of few meters [14]–[16]. Several ranging methods have been proposed to mitigate the clock drifts for high-precision localization. Before revisiting existing methods, we introduce some terms for ease of illustration.

A ranging network is shown in Fig. 1 (a). Each node has two modes of operating: the *active mode* and the *silent mode*, where the operating mode is fixed in one ranging period but can be different across different ranging periods. For ease of expression, we refer to a node that works in the active mode as an active node and that works in the silent mode as a silent node. Active nodes transmit ranging signals and receive signals from other active nodes, while silent nodes only receive ranging signals from active nodes. In this network, two kinds of range parameters, the *absolute ranges* and the *differential ranges*, are to be estimated. Specifically, absolute ranges are defined as the distances between two nodes, while differential ranges are the distance differentials between two node pairs. For clarity, we plot Fig. 1 (b) to explicitly illustrate the relationship between the absolute range and the differential

range. In parallel to ranges, the ranging methods are divided into two categories, i.e., *active ranging* and *silent ranging*. The goal of active ranging is to determine the absolute pairwise ranges between active nodes, and that of silent ranging focuses on determining the differential ranges between silent-active node pairs.

A. Related Works

The most popular active ranging method is the two-way ranging (TWR) method [17], in which each node transmits a signal and the distance is estimated by measuring the round-trip time-of-flight (ToF) [18]. However, due to clock drifts, directly implementing TWR will lead to meter-level ranging errors [19]–[21], which is unacceptable for high-precision localization. Many TWR variations have been proposed to resolve the clock drifts, such as the single-sided TWR [20], the alternative double-sided TWR (AltDS-TWR) [20], the double TWR [22], the double-sided TWR [23], the asymmetric double-sided TWR [24], the symmetric double-sided TWR [25], the symmetric multi-way ranging [26], and the network-based TWR (NB-TWR) [27]. Theoretical analyses and field tests have shown that AltDS-TWR in [20] is the most robust one to clock drifts [28]–[30]. Apart from accuracy, spectral resource consumption is also an important aspect when evaluating a ranging method. It is shown that the number of required ranging signals of methods in [19]–[25] are square of the network scale, meaning the signal overhead will grow dramatically as the number of network nodes increases. For example, three ranging signals are required by AltDS-TWR to measure the distance between two active nodes, while 135 signals are required for the network within 10 active nodes. Since mass signal transmissions always mean long latency, large energy consumption, and heavy hardware resource occupation [13], optimizing ranging methods to reduce signal overhead is worth further investigation.

On the other hand, since silent nodes do not produce ranging signal overhead, assigning some nodes working in silent mode is an effective way for large-scale networks to save spectral resources [31], [32]. Note that, since silent nodes do not participate in signal transmission, the absolute ranges between silent nodes and other nodes cannot be directly measured [31]–[33] and only the differential ranges between silent and active node pairs can be measured. Therefore, different from active ranging, silent ranging is designed to determine the differential ranges between silent and active node pairs via measuring time-difference-of-flight (TDoF) [33]. There have been several works on silent ranging, including the network-based passive ranging (NB-PR) [27], the passive extended ranging (PER) [33], the sequential time-difference-of-arrival (S-TDOA) [31], and the passive ranging (PR) method in [32], among which the best-performing one is the PER [33]. As for ranging efficiency, since silent ranging methods attach themselves to active ranging and only available to particular protocols, these methods are inapplicable to the designed protocol in this paper. Moreover, most existing silent ranging methods work relying on anchors with known positions [31]–[33], while our work mainly focuses anchor-free networks.

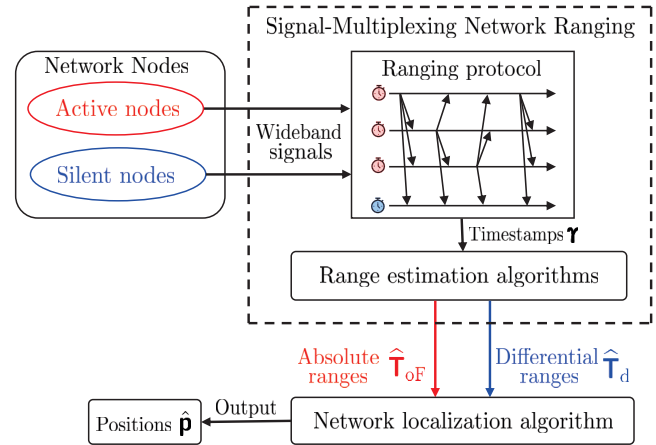


Fig. 2. The proposed localization framework, which achieves high-efficiency network ranging via signal-multiplexing.

B. Our Contributions

In this paper, we propose a high-efficiency localization framework, which fully mitigates the clock drift effect using a minimum number of signal transmissions. Our contributions are summarized as follows.

- We establish a localization framework for networks in presence of clock drifts (Fig. 2), which consists of a ranging method with a minimum number of signal transmissions and a localization algorithm achieving high-accuracy relative positioning.
- We propose a network ranging method named SM-NR, which only requires the number of signal transmissions being linear with the network scale and effectively eliminates clock drifts within designed maximum likelihood (ML) ranging estimators.
- We develop a high-precision localization algorithm for relative network localization. Theoretical analyses and simulation results demonstrate that the developed localization algorithm provides precise location awareness with low signal overhead.

C. Organizations and Notations

The rest of the paper is organized as follows. In Section II, we briefly introduce the system model and the considered ranging problem. The proposed ranging method SM-NR is detailed in Section III and its performance is analyzed in Section IV. We present the network localization algorithm in V. Numerical simulation results are provided in Section VI, and finally the conclusions are summarized in Section VII.

Notation: The notation \mathbb{R} denotes the set of real numbers; variables, vectors, and matrices are written as italic letters x , bold italic letters \mathbf{x} , and bold capital italic letters \mathbf{X} , respectively; random variables, random vectors, and random matrices are written as sans serif letter x , bold letters \mathbf{x} , and bold capital letters \mathbf{X} , respectively; the bold letters with hats $\hat{\mathbf{X}}$ denote the estimators; $\mathbb{E}_{\mathbf{z}}\{\cdot\}$ is the expectation operator with respect to the random vector \mathbf{z} ; $\text{Var}_{\mathbf{z}}\{\cdot\}$ is the variance operator with respect to the random vector \mathbf{z} ; $\|\cdot\|$ denotes the

Euclidean norm of its argument; superscript $[\cdot]^T$ represents the transpose of the argument; $\mathbf{1}_L$ indicates an L -length vector with all elements being 1.

II. PRELIMINARY

In this section, we introduce the system model and formulate the ranging problem.

A. Nodes in Asynchronous Network

Consider an N -node asynchronous network with N_a nodes working in active mode and N_s nodes working in silent mode, where $N \equiv N_a + N_s$. Without loss of generality, let $\mathcal{N}_a \triangleq \{1, 2, \dots, N_a\}$ and $\mathcal{N}_s \triangleq \{N_a + 1, N_a + 2, \dots, N_a + N_s\}$ denote the index sets of active and silent nodes, respectively, and $\mathcal{N} \triangleq \mathcal{N}_a \cup \mathcal{N}_s$ denote the index set of all nodes. The 2-D position of node n ($n \in \mathcal{N}$) is denoted by $\mathbf{p}_n = [x_n \ y_n]^T \in \mathbb{R}^2$ and the position vector of all nodes is defined as

$$\mathbf{p} = [\mathbf{p}_1^T \ \mathbf{p}_2^T \ \dots \ \mathbf{p}_N^T]^T \in \mathbb{R}^{2N}. \quad (1)$$

In this paper, the node positions \mathbf{p} will be estimated according to geometric relationships based on range estimations.¹ Particularly, we focus on the centralized framework where the measurements are processed in a fusion center, and we will further extend the proposed framework for distributed networks in Section III-C.

B. Ranges to Be Measured in Network

In the investigated network consisting of both active and silent nodes, two kinds of range parameters, the *absolute ranges* and the *differential ranges*, are to be estimated, which are defined as follows:

- **Absolute ranges:** The distance between two nodes. Let d_{n_1, n_2} and $T_{\text{OF}}(n_1, n_2)$ respectively denote the absolute range and the ToF between nodes n_1 and n_2 , which satisfies $d_{n_1, n_2} = cT_{\text{OF}}(n_1, n_2)$ where c is the light speed. For a network with N_a active nodes and N_s silent nodes, only $\binom{N_a}{2}$ absolute ranges among N_a active nodes can be estimated.
- **Differential ranges:** The distance differential between two node pairs. In particular, we focus on the differential range between two silent-active node pairs. For example, for silent-active node pairs (i, k) and (j, k) with node k being a silent node and nodes i and j being active nodes, the differential range is defined as

$$R_{k; i, j} = d_{i, k} - d_{j, k}. \quad (2)$$

It satisfies $R_{k; i, j} = cT_d(k; i, j)$, where $T_d(k; i, j)$ is the TDoF between node pairs (i, k) and (j, k) , defined by

$$T_d(k; i, j) = T_{\text{OF}}(i, k) - T_{\text{OF}}(j, k). \quad (3)$$

For a network with N_a active nodes and N_s silent nodes, there are $N_s \binom{N_a}{2}$ differential ranges to be estimated in total.

¹The node positions also can be estimated based on the direction information such as angle-of-departure and angle-of-arrival by equipping antenna arrays [34]–[36]. Since clock drifts have limited effects on this kind of information, we thus focus on eliminating clock drifts on distance information in this paper.

C. Clock Model

When an active node transmits a ranging signal, each node will capture a timestamp which characterizes the sending time (itself) or receiving time of the signal. Let $t_m^{(n)}$ denote the true time of the m -th timestamp captured by node n ($n \in \mathcal{N}$). However, due to non-ideal clocks, the timestamp measurement $\Upsilon_m^{(n)}$ is modeled as [13]–[16]

$$\Upsilon_m^{(n)} = (1 + e^{(n)})t_m^{(n)} + \theta^{(n)} = k^{(n)}t_m^{(n)} + \theta^{(n)} \quad (4)$$

where $\theta^{(n)}$, $e^{(n)}$, and $k^{(n)}$ denote the time offset associated with the clock boot time, the clock frequency deviation, and the clock skew of the n -th node, respectively [13]. We have the following assumption on the clock frequency deviation $e^{(n)}$.

Assumption 1: According to the IEEE 802.15.4a standard [37], the clock frequency deviation $e^{(n)}$ is assumed as a normalized random variable bounded by $[-e_{\text{max}}, +e_{\text{max}}]$ and independent of each other [37]–[39]. Moreover, since the ranging period is usually very short (several milliseconds), the clock frequency deviations $e^{(n)}$ is assumed as time-invariant within one ranging period. This is nevertheless a standard assumption in most prior works [28]–[33].

Let \mathbf{e} denote the overall vector of the clock frequency deviation parameter $e^{(n)}$, given by

$$\mathbf{e} = [e^{(1)} \ e^{(2)} \ \dots \ e^{(N)}]^T. \quad (5)$$

Apart from clock drifts, in practice, the timestamp $\Upsilon_m^{(n)}$ is also influenced by measurement errors, where the influential factors include the hardware impairments, non-line-of-sight (NLOS) paths, clock jitter,² received signal-to-noise ratio (SNR), timestamp detection method and etc [38], [39], [44]–[46]. In this case, we model the timestamp measurement as

$$\Upsilon_m^{(n)} = k^{(n)}t_m^{(n)} + \theta^{(n)} + w_m^{(n)} \quad (6)$$

where $w_m^{(n)}$ denotes the measurement error.³

In this paper, we aim to establish an efficient localization framework for networks under the influences of non-ideal clocks. Particularly, the ranging method is optimized to effectively mitigate the clock effects with the minimum of ranging signal transmissions. The clock model in (4) is first considered, and further the clock model in (6) is theoretically analyzed and numerically evaluated in Section IV-C and Section VI-C, respectively.

III. SIGNAL-MULTIPLEXING NETWORK RANGING METHOD

The proposed network ranging method is presented in this section, including a ranging protocol, an ML ToF estimator, and an TDoF estimator.

²Note that, compared with clock drifts, the impact of clock jitters is negligible [40]–[42]. For example, for a standard SG2016 crystal oscillator working at 20 MHz (± 100 ppm), the clock jitter is within ± 0.3 ps [43]. Then, if the ranging process takes 10 ms in total, the timing error caused by clock drifts is about 1 μ s, while that caused by clock jitter is 60 ns in the worst case [43]. Besides, the impact of clock jitters can be viewed as a part of timestamp measurement errors, as shown in (6).

³This paper focuses on eliminating the impact of clock drifts for network localization and the specific values of parameters in clock model (6) depend on application scenarios, including but not limit to 5G ecosystem or WiFi.

A. Ranging Protocol

For ease of illustration, we first consider a fully connected network, where each ranging signal can be received by all nodes in the network with line-of-sight (LOS) paths. In later Section III-C, we will tackle partially connected networks to remove this assumption.

An illustration of the proposed ranging protocol is shown in Fig. 3, where the order of signal transmissions is pre-set. Specifically, an active node launches the ranging process by transmitting the first ranging signal.⁴ After a preset delay, another active node transmits the second ranging signal. By analogy, each active node will transmit a ranging signal in turn, and the first-transmit node completes the ranging process by transmitting the last ranging signal. For a network with N_a active nodes, this ranging protocol requires $N_a + 1$ ranging signals in total, which is shown as the minimal number of signal transmissions for high-precision ranging in Section III-D. Under the assumption that each ranging signal can be received by all nodes in the network, $\binom{N_a}{2}$ absolute ranges and $N_s \binom{N_a}{2}$ differential ranges can be measured, denoted by

$$T_{\text{oF}} := \{T_{\text{oF}}(i, j) \mid i, j \in \mathcal{N}_a\} \quad (7)$$

$$T_{\text{d}} := \{T_{\text{d}}(k; i, j) \mid i, j \in \mathcal{N}_a, k \in \mathcal{N}_s\}. \quad (8)$$

Without loss of generality, assume the ranging signal transmission order is the node number.

Let \mathbf{t} and $\boldsymbol{\Upsilon}$ denote all the true timestamps and the observed timestamps, given by

$$\begin{aligned} \mathbf{t} &= [(\mathbf{t}^{(1)})^T (\mathbf{t}^{(2)})^T \dots (\mathbf{t}^{(N)})^T]^T \\ \boldsymbol{\Upsilon} &= [(\boldsymbol{\Upsilon}^{(1)})^T (\boldsymbol{\Upsilon}^{(2)})^T \dots (\boldsymbol{\Upsilon}^{(N)})^T]^T \end{aligned} \quad (9)$$

where $\mathbf{t}^{(n)}$ and $\boldsymbol{\Upsilon}^{(n)}$ are the true and the observed timestamps by node n , respectively, given by

$$\begin{aligned} \mathbf{t}^{(n)} &= [t_1^{(n)} t_2^{(n)} \dots t_M^{(n)}]^T \\ \boldsymbol{\Upsilon}^{(n)} &= [\Upsilon_1^{(n)} \Upsilon_2^{(n)} \dots \Upsilon_M^{(n)}]^T \end{aligned} \quad (10)$$

in which $M := N_a + 1$ is the total number of transmitted ranging signals during the measuring period. All the timestamp observations are then transmitted to a fusion center for joint processing to determine the ToFs and the TDoFs. Note that there is no need to transmit timestamps using wideband ranging signals, instead, low-cost wireless methods such as Wifi, Bluetooth, and Zigbee are preferred.

Before introducing our range estimation algorithm, we first discuss an intuitive ToF estimator to show the serious impact of clock drifts on ranging accuracy. As the basis of derivation, we define the notation $D_{i,j}^{(n)}$ as follows.

Definition 1: Let n ($n \in \mathcal{N}$) denote an arbitrary node, i and j denote two active nodes with $i < j$. Notation $D_{i,j}^{(n)} = t_j^{(n)} - t_i^{(n)}$ denotes the true time interval at node n between the timestamps made by active nodes i and j . For $D_{i,j}^{(n)}$, the clock offset factor $\theta^{(n)}$ in clock model (4) and (6) is canceled out.

⁴The selection of the first node is flexible. For example, polling strategy is a promising scheme to find out the best initial node that links as many nodes as possible, so that the proposed ranging method can work efficiently.

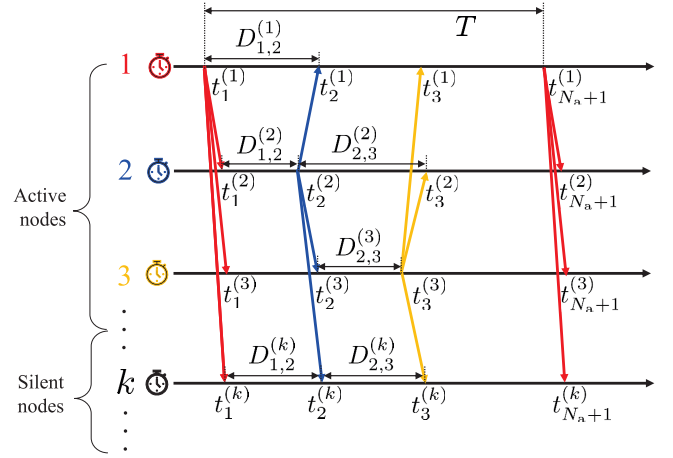


Fig. 3. Illustration of the ranging protocol of the proposed SM-NR method, where each black horizontal arrow line denotes the clock timeline, and the colored arrow lines denote ranging signal transmissions. Active node 1, 2 and 3 transmit the first, the second, and the third ranging signal, respectively and node k is a silent node.

As shown in Fig. 3, $D_{i,j}^{(i)} = t_j^{(i)} - t_i^{(i)}$ characterizes the round-trip time (RTT) and $D_{i,j}^{(j)} = t_j^{(j)} - t_i^{(j)}$ represents the waiting time at node j [47]. Thus, the ToF between i and j satisfies

$$T_{\text{oF}}(i, j) = \frac{1}{2} (D_{i,j}^{(i)} - D_{i,j}^{(j)}). \quad (11)$$

However, due to clock errors, $D_{i,j}^{(n)}$ is not available and only its observation, denoted as $\Omega_{i,j}^{(n)}$ which satisfies $\Omega_{i,j}^{(n)} := \Upsilon_j^{(n)} - \Upsilon_i^{(n)}$, can be obtained. Inspired by (11), an intuitive ToF estimator without mitigating clock drifts is given by

$$\widehat{T}'_{\text{oF}}(i, j) := \frac{1}{2} (\Omega_{i,j}^{(i)} - \Omega_{i,j}^{(j)}), \quad (12)$$

of which the estimation error under model (4) can be derived as

$$\begin{aligned} E'(i, j) &:= \widehat{T}'_{\text{oF}}(i, j) - T_{\text{oF}}(i, j) \\ &= \frac{1}{2} (\Omega_{i,j}^{(i)} - \Omega_{i,j}^{(j)}) - \frac{1}{2} (D_{i,j}^{(i)} - D_{i,j}^{(j)}) \\ &= \frac{1}{2} (e^{(i)} - e^{(j)}) D_{i,j}^{(j)} + e^{(i)} T_{\text{oF}}(i, j) \end{aligned} \quad (13)$$

which characterizes the effect of clock drifts $e^{(n)}$. The estimation error $E'(i, j)$ is significant. For example, when $e^{(i)}, e^{(j)} \in [-20, +20]$ ppm, $T_{\text{oF}}(i, j) = 100$ ns (i.e. 30 m), and $D_{i,j}^{(j)} = 1$ ms, the estimation error will be larger than 20 ns in the worst case, resulting in an unacceptable range error around 6 m. Therefore, to achieve high-accuracy ranging, the clock drifts should be effectively mitigated.

B. ML ToF and TDoF Estimators

Using the protocol in Fig. 3, we next show how the proposed SM-NR method mitigates clock drifts. We first introduce active ranging, i.e., ToF estimation. With the timestamp observation $\boldsymbol{\Upsilon}$ in (10), the ML ToF estimator $\widehat{T}_{\text{oF}}^*$ is formulated as

$$\widehat{T}_{\text{oF}}^* = \underset{T_{\text{oF}}}{\operatorname{argmax}} \ell_e(\boldsymbol{\Upsilon}; T_{\text{oF}}) \quad (14)$$

where $\ell_e(\cdot; \cdot)$ denotes the likelihood function with respect to random vector \mathbf{e} in (5). To solve (14), we define the following term.

Definition 2: The *synchronization time* is defined as the transmitted time interval between two signals from the first node, denoted as T . Ideally, $T = t_{N_a+1}^{(n)} - t_1^{(n)}$ holds for any node $n \in \mathcal{N}$, as shown in Fig. 3.

Based on clock model (4), it can be verified that the following relationships hold:

$$\mathsf{T}^{(n_1)} = k_{n_1} T \quad (15a)$$

$$\frac{\mathsf{T}^{(n_1)}}{\mathsf{T}^{(n_2)}} = \frac{k^{(n_1)} T}{k^{(n_2)} T} = \frac{k^{(n_1)}}{k^{(n_2)}}, \quad \text{for } n_1, n_2 \in \mathcal{N} \quad (15b)$$

where $\mathsf{T}^{(n)}$ represents the synchronization time T observed by node $n \in \mathcal{N}$, i.e.,

$$\mathsf{T}^{(n)} := \Upsilon_{N_a+1}^{(n)} - \Upsilon_1^{(n)}.$$

From (11) and (15), we note that the ToF between active nodes i and j naturally satisfies

$$\begin{aligned} T_{\text{oF}}(i, j) &= \frac{1}{2} \left(\frac{T}{k^{(i)} T} k^{(i)} D_{i,j}^{(i)} - \frac{T}{k^{(j)} T} k^{(j)} D_{i,j}^{(j)} \right) \\ &= \frac{T}{2} \left(\frac{\Omega_{i,j}^{(i)}}{\mathsf{T}^{(i)}} - \frac{\Omega_{i,j}^{(j)}}{\mathsf{T}^{(j)}} \right). \end{aligned} \quad (16)$$

Then, based on (16) and using functional invariance, the ML ToF estimation $\hat{\mathsf{T}}_{\text{oF}}^*(i, j)$ can be derived by replacing the synchronization time T in (16) with its ML estimator, i.e.,

$$\hat{\mathsf{T}}^* = \underset{T}{\operatorname{argmax}} \ell_e(\boldsymbol{\Upsilon}; T) \quad (17)$$

To sum up, the ML ToF estimator $\hat{\mathsf{T}}_{\text{oF}}^*$ in (14) is derived in the following proposition.

Proposition 1: For the clock frequency deviation $e^{(n)}$ with the probability density function (PDF) $h_{e^{(n)}}$, the ML ToF estimators defined in (14) can be described as

$$\hat{\mathsf{T}}_{\text{oF}}^*(i, j) = \frac{\hat{\mathsf{T}}^*}{2} \left(\frac{\Omega_{i,j}^{(i)}}{\mathsf{T}^{(i)}} - \frac{\Omega_{i,j}^{(j)}}{\mathsf{T}^{(j)}} \right), \quad \text{for all } i, j \in \mathcal{N}_a \quad (18)$$

wherein $\hat{\mathsf{T}}^*$ denotes the ML estimator of the synchronization time T , given by

$$\hat{\mathsf{T}}^* = \underset{T}{\operatorname{argmax}} \prod_{n=1}^N h_{e^{(n)}}(\mathsf{T}^{(n)}; T). \quad (19)$$

Proof: Since the clock at each node is independent, (17) can be rewritten as

$$\begin{aligned} \hat{\mathsf{T}}^* &= \underset{T}{\operatorname{argmax}} \ell_e(\mathsf{T}^{(1)}, \dots, \mathsf{T}^{(N)}; T) \\ &= \underset{T}{\operatorname{argmax}} \prod_{n=1}^N h_{e^{(n)}}(\mathsf{T}^{(n)}; T). \end{aligned} \quad (20)$$

Given the distribution of $e^{(n)}$, the exact ML ToF estimation can be obtained by substituting the PDF $h_{e^{(n)}}$ into (19) and solving the optimization problem. \square

Remark 1: From (19), we note that the ML estimator $\hat{\mathsf{T}}^*$ is determined by the distribution of clock frequency deviation

parameters, which highly depend on the physical characteristics of clocks [13], [38]. The IEEE 802.15.4a standard only assumes that the clock frequency deviation $e^{(n)}$ is a random variable bounded by $[-e_{\max}, +e_{\max}]$, while the specific probability distribution is not provided [37]. Similar to [21], [30], [39], here we take the uniform distribution as an example. Under the assumption that the clock frequency deviation is uniformly distributed in the interval $[-e_{\max}, +e_{\max}]$, the ML ToF estimator of the synchronization time T takes the form of

$$\hat{\mathsf{T}}^* = \frac{\max_{n \in \mathcal{N}} \{\mathsf{T}^{(n)}\}}{1 + e_{\max}}. \quad (21)$$

Next, consider silent ranging. As shown in Fig. 3, since silent nodes do not participate in ranging signal transmission, no such round trip related to silent nodes exists. Thus, the absolute distances between silent nodes and other nodes cannot be measured [31]–[33]. As an alternative, we estimate the differential ranges, which characterize the distance difference between two silent-active node pairs.

From Fig. 3, we note that the following relationship holds for arbitrary $i, j \in \mathcal{N}_a$ and $k \in \mathcal{N}_s$:

$$T_{\text{oF}}(i, j) + D_{i,j}^{(j)} + T_{\text{oF}}(j, k) = T_{\text{oF}}(i, k) + D_{i,k}^{(k)}. \quad (22)$$

Combining (3), (22) and (11), we have

$$T_d(k; i, j) = \frac{1}{2} D_{i,j}^{(j)} + \frac{1}{2} D_{i,j}^{(i)} - D_{i,k}^{(k)}. \quad (23)$$

Then, using the same method as the ToF estimators, we obtain the ML estimators of the TDoFs, as shown in the following proposition.

Proposition 2: For the clock deviation parameter $e^{(n)}$ with the PDF $h_{e^{(n)}}(\cdot)$, the ML estimation of the TDoF is given by

$$\begin{aligned} \hat{\mathsf{T}}_d^*(k; i, j) &= \frac{\hat{\mathsf{T}}^*}{2\mathsf{T}^{(j)}} \Omega_{i,j}^{(j)} + \frac{\hat{\mathsf{T}}^*}{2\mathsf{T}^{(i)}} \Omega_{i,j}^{(i)} - \frac{\hat{\mathsf{T}}^*}{\mathsf{T}^{(k)}} \Omega_{i,j}^{(k)}, \\ &\quad \text{for } i, j \in \mathcal{N}_a \text{ and } k \in \mathcal{N}_s \end{aligned} \quad (24)$$

where $\hat{\mathsf{T}}^*$ is given in (19).

C. Extension to Networks With Partial Observations

We extend the above ranging method to address the cases where only partial timestamp observations are available, including partially connected networks and distributed networks.

1) *Partially Connected Networks:* Without LOS paths, the absolute range between two nodes is unavailable and we refer to these two nodes as disconnected.

Firstly, we discuss the case where all nodes have LOS links with node 1, which means that the synchronization time T can be well observed by all nodes. Let $\tilde{\boldsymbol{\Upsilon}}$ denote the whole network timestamp observation, which takes the form of

$$\tilde{\boldsymbol{\Upsilon}} = \left[(\tilde{\boldsymbol{\Upsilon}}^{(1)})^T \ (\tilde{\boldsymbol{\Upsilon}}^{(2)})^T \ \dots \ (\tilde{\boldsymbol{\Upsilon}}^{(N)})^T \right]^T$$

where $\tilde{\boldsymbol{\Upsilon}}^{(n)} = \left[\Upsilon_1^{(n)} \ \Upsilon_2^{(n)} \ \dots \ \Upsilon_{\text{card}(\mathcal{N}^{(n)})}^{(n)} \right]^T$ denotes the observed timestamps at node n . Here, $\mathcal{N}^{(n)}$ denotes an active-node set, where each element can build a round trip with node n through LOS paths, and $\text{card}(\cdot)$ denotes the number of

elements in the argument. Under this circumstance, the ML estimator of the synchronization time T in (17) becomes

$$\tilde{T} = \operatorname{argmax}_T \ell_e(\tilde{\mathbf{r}}; T). \quad (25)$$

In particular, when the clock frequency deviation is uniformly distributed in $[-e_{\max}, +e_{\max}]$, the ML ToF estimation of T can be described as

$$\tilde{T} = \frac{\max_{n \in \tilde{\mathcal{N}}} \{\Upsilon^{(n)}\}}{1 + e_{\max}}$$

where $\tilde{\mathcal{N}}$ denotes the node set, of which the elements can receive ranging signals from node 1. At this time, if an active node i can receive signals from node 1, the ML ToF estimation between active nodes i and j ($j \in \mathcal{N}^{(i)}$) is given by⁵

$$\tilde{T}_{\text{ToF}}(i, j) = \frac{\tilde{T}}{2} \left(\frac{\Omega_{i,j}^{(i)}}{\Upsilon^{(i)}} - \frac{\Omega_{i,j}^{(j)}}{\Upsilon^{(j)}} \right), \quad \text{for } j \in \mathcal{N}^{(i)}. \quad (26)$$

Similarly, for silent node k connecting with node 1, the ML TDoF estimation for it with active nodes i and j ($i, j \in \mathcal{N}^{(k)}$) is given by

$$\tilde{T}_{\text{d}}(k; i, j) = \frac{\tilde{T}}{2\Upsilon^{(j)}} \Omega_{i,j}^{(j)} + \frac{\tilde{T}}{2\Upsilon^{(i)}} \Omega_{i,j}^{(i)} - \frac{\tilde{T}}{\Upsilon^{(k)}} \Omega_{i,j}^{(k)}, \quad \text{for } i, j \in \mathcal{N}^{(k)}. \quad (27)$$

Secondly, we discuss the case when a node n ($n \in \mathcal{N}/1$) connects with node 1 but only receives NLOS signals from node 1. Denote two timestamp observations regarding the first NLOS path as $\Upsilon_1^{(n)}$ and $\Upsilon_{N_a+1}^{(n)}$. We note that the relationship $\Upsilon_{N_a+1}^{(n)} - \Upsilon_1^{(n)} = k_n T$ still holds.⁶ Thus, the clock drifts of node n still can be mitigated using the proposed ranging method. In this case, although the range estimation between node n and 1 is unreliable due to the lack of LOS path, the ranges between node n and the nodes, which have LOS paths connecting with node n , can still be reliably estimated.

Thirdly, we discuss the case where node n does not connect with node 1. In such circumstances, the ranging method fails due to lacking observations of synchronization time T . Therefore, we address the network localization by cascaded broadcasting, which can be achieved in a multi-hop way. For example, consider a network within three active nodes, where the communication link between nodes 1 and 3 does not exist. We can first perform the proposed ranging method between nodes 1 and 2. Then, we view node 2 as the first-transmit node and perform the ranging method between nodes 2 and 3.

2) *Distributed Networks*: Furthermore, we extend the above centralized ranging method for distributed realization, where the ranging task is finished by several subtasks. For example, denote the index set of subnetwork k as \mathcal{N}_k , and then the ML

⁵For node $j' \notin \mathcal{N}^{(i)}$, since the RTT $D_{i,j'}^{(i)}$ in (11) cannot be acquired, the absolute range between i and j' is not available.

⁶Since the ranging period is usually very short (several milliseconds), the propagation environments during the whole ranging period can be viewed as unvaried. Thus, the propagation time of the two NLOS signals from node 1 are almost equal and $\Upsilon_{N_a+1}^{(n)} - \Upsilon_1^{(n)} = k_n T$ holds.

Algorithm 1 Signal-Multiplexing Network Ranging (SM-NR)

Input: An N -node network with active node set \mathcal{N}_a and silent node set \mathcal{N}_s ;

Output: All absolute range estimations $\hat{d}_{i,j}$ and differential range estimations $\hat{R}_{k;i,j}$, where $i, j \in \mathcal{N}_a$ and $k \in \mathcal{N}_s$.

- 1: $n \leftarrow 1$;
 - 2: **while** $n < N_a + 1$ **do**
 - 3: Node n broadcasts a ranging signal;
 - 4: $n \leftarrow n + 1$;
 - 5: **end while**
 - 6: Node 1 broadcasts a ranging signal again;
 - 7: The computing center estimates all ToFs and TDoFs by (18) and (24), respectively;
 - 8: Calculate absolute ranges $\hat{d}_{i,j}$ and differential ranges $\hat{R}_{k;i,j}$ according to (29);
 - 9: **return** All absolute range estimations $\hat{d}_{i,j}$ and differential range estimations $\hat{R}_{k;i,j}$.
-

TABLE I

REQUIRED RANGING SIGNALS OF DIFFERENT RANGING SCHEMES

Active ranging methods	Required ranging signals
AltDS-TWR [20]	$\frac{3}{2} N_a(N_a - 1)$
NB-TWR [27]	$N_a + 1$
SM-NR	$N_a + 1$

estimation of the synchronization time T in (17) is redefined as

$$\tilde{T}_k = \operatorname{argmax}_T \ell_e(\{\tilde{\mathbf{r}}_n, n \in \mathcal{N}_k\}; T). \quad (28)$$

After solving optimization problem (28) with certain probability density functions, \tilde{T}_k is obtained. Subsequently, replacing \tilde{T} in (26) and (27) with \tilde{T}_k , the ToF and TDoF parameters in subnetwork k can be estimated in a distributed manner.

D. Summary of the SM-NR Method

We summarize the proposed SM-NR method in Algorithm 1 and conclude its merit as follows.

In the presence of clock drifts, through using the SM-NR, the signal overhead for realizing high-precision network ranging has been significantly reduced. Specifically, for an asynchronous network with N_a active nodes and N_s silent nodes, the proposed SM-NR method only requires $N_a + 1$ ranging signals to measure all $\binom{N_a}{2}$ ToFs and $N_s \binom{N_a}{2}$ TDoFs. In comparison, to achieve the same goal, $3 \binom{N_a}{2}$ ranging signals are required by employing the combination of the popular active ranging method AltDS-TWR [20] and silent ranging method PER [33]. To clearly show the efficiency enhancement, we compare the proposed SM-NR with the existing widely-adopted ranging methods AltDS-TWR [20]

and NB-TWR⁷ [27], and present their ranging signal overhead in Table I. It is shown that the signal overhead of the AltDS-TWR is $\mathcal{O}(N_a^2)$, while those required by our works, i.e., the NB-TWR [27] and the SM-NR, are $\mathcal{O}(N_a)$. Particularly, we prove that SM-NR has used the minimum number of ranging signals in the following proposition.

Proposition 3: The proposed SM-NR method requires $N_a + 1$ ranging signals for measuring all ranges in a network with N_a active nodes, while $N_a + 1$ is actually the minimum number to achieve the goal of high-accuracy ranging.

Proof: Since each active node transmits at least one signal (otherwise it degenerates to a silent node), the number of required ranging signals is no less than N_a . While if all active nodes only transmit once, none node generates a synchronization time T for clock drift elimination and thus only the rough ToF estimation in (12) can be obtained, of which the performance cannot meet the demand of high-precision network ranging. As a result, $N_a + 1$ is the minimum number of signal transmission for high-precision network ranging. \square

Therefore, from the perspective of resource-saving, the proposed SM-NR method is much more efficient than the state-of-art methods, especially in large-scale networks. In the next section, the precision merit of the SM-NR will be shown, which confirms that clock drifts can be fully mitigated by the proposed ML estimators.

IV. PERFORMANCE ANALYSIS

In this section, we evaluate the precision of the ToF and TDoF obtained via the proposed SM-NR method. Here, we assume the clock frequency deviation $e^{(n)}$ is a uniform distributed variable, i.e., $e^{(n)} \sim \mathcal{U}(-e_{\max}, e_{\max})$, which is similar to [21], [30], [39].

Recall that $d_{i,j}$ and $R_{k;i,j}$ ($i, j \in \mathcal{N}_a$, $k \in \mathcal{N}_s$) denote the absolute range and the differential range between nodes i, j and node pairs (i, k) and (j, k) and are estimated from the ToF $T_{\text{of}}(i, j)$ and the TDoF $T_d(k; i, j)$, respectively, given by

$$\hat{d}_{i,j} = c \cdot \hat{T}_{\text{of}}(i, j) \quad \text{and} \quad \hat{R}_{k;i,j} = c \cdot \hat{T}_d(k; i, j) \quad (29)$$

where $\hat{T}_{\text{of}}(i, j)$ denotes the estimation of $T_{\text{of}}(i, j)$, $\hat{T}_d(k; i, j)$ denotes the estimation of $T_d(k; i, j)$, and c denotes the light speed. Then, the measurement errors of $d_{i,j}$ and $R_{k;i,j}$ are defined as

$$\omega_{i,j} = \hat{d}_{i,j} - d_{i,j} \quad \text{and} \quad \omega_{k;i,j} = \hat{R}_{k;i,j} - R_{k;i,j}. \quad (30)$$

A. Precision of Absolute Range Estimations

We first evaluate the worst-case performance of the absolute range estimation, and we obtain the following proposition.

Proposition 4: The worst-case performance of the absolute range estimation $\hat{d}_{i,j}$ in (29) can be described by

$$\max_e \{|\omega_{i,j}|\} = \frac{2e_{\max}}{1 + e_{\max}} d_{i,j} \quad (31)$$

⁷The NB-TWR and the NB-PR are our parallel works published as a conference paper [27], which also can measure all $\binom{N_a}{2}$ ToFs and $N_s \binom{N_a}{2}$ TDoFs within $N_a + 1$ ranging signals. However, their precision are worse than the SM-NR in this paper, as shown in Section VI.

where $\omega_{i,j}$, \mathbf{e} and e_{\max} are defined in (30), (5) and (4), respectively.

Proof: It can be verified that the estimation error of $\hat{d}_{i,j}$ takes the form of

$$\begin{aligned} \omega_{i,j} &\stackrel{(a)}{=} c \frac{\hat{T}^*}{2} \left(\frac{\Omega_{i,j}^{(i)}}{T^{(i)}} - \frac{\Omega_{i,j}^{(j)}}{T^{(j)}} \right) - d_{i,j} \stackrel{(b)}{=} c \frac{\hat{T}^*}{T} T_{\text{of}}(i, j) - d_{i,j} \\ &\stackrel{(c)}{=} \left(\frac{\hat{T}^*}{T} - 1 \right) d_{i,j} \stackrel{(d)}{=} \left(\frac{\max_{n \in \mathcal{N}} \{T^{(n)}\}}{T(1 + e_{\max})} - 1 \right) d_{i,j} \quad (32) \end{aligned}$$

where (a) holds according to (18), (b) is obtained from (16), (c) holds since $cT_{\text{of}}(i, j) \equiv d_{i,j}$, and (d) is obtained based on (21). Then, the maximum absolute value of (32) satisfies (31). \square

From (32) we note that, compared with the intuitive estimator in (12), the ML estimator of the proposed SM-NR has fully mitigated the clock drifts. To see this, consider the same evaluation setups in Section III-A, i.e., $e \in [-20, +20]$ ppm and $T_{\text{of}}(i, j) = 100$ ns (i.e. 30 m). Then, according to (31), the worst-case value of $\omega_{i,j}$ is about 1.2 mm, which is much lower than the 6-meter worst-case error shown in (12) in Section III-A.

Actually, the worst-case error (31) achieves only when $e^{(n)} = -e_{\max}$ for all node $n \in \mathcal{N}$, which rarely happens in practice, especially when the network is large. Thus, we further investigate the statistical performance of error $\omega_{i,j}$ to comprehensively evaluate the proposed SM-NR method, and we obtain the following proposition.

Proposition 5: The root mean square error (RMSE) of the absolute range estimation $\hat{d}_{i,j}$ is given by

$$\text{RMSE}_{i,j} = \sqrt{\mathbb{E}_e \{\omega_{i,j}^2\}} = \sqrt{\frac{8}{(N+1)(N+2)} \frac{e_{\max} d_{i,j}}{1 + e_{\max}}}. \quad (33)$$

Proof: See Appendix A. \square

For comparison, the RMSEs of the proposed SM-NR and the widely-adopted active ranging methods [20], [27] are summarized in Table II. From Table I and Table II, we note that the proposed ToF estimator achieves the same order of magnitude accuracy as the state-of-art active ranging methods, but the signal overhead is significantly lower. Moreover, different from the others, the RMSE of the ML estimator $\hat{d}_{i,j}$ is inversely proportional to the network size N , which indicates that increasing the network size can enhance the precision performance. This is because the more observations of synchronization time T , the more accurate the ML estimator of T will be, as in (20). Particularly, as N increases, the RMSE of the SM-NR gradually approaches zero and we conclude that the proposed SM-NR provides a high-efficiency way to realize effective ranging in the presence of clock drifts, especially for large-scale networks.

B. Precision of Differential Range Estimations

We evaluate the performance of differential range estimators. Note that the error of $\hat{R}_{k;i,j}$ in (29) can be derived as

$$\omega_{k;i,j} = \left(\frac{\hat{T}^*}{T} - 1 \right) R_{k;i,j} = \left(\frac{\max_{n \in \mathcal{N}} \{T^{(n)}\}}{T(1 + e_{\max})} - 1 \right) R_{k;i,j} \quad (34)$$

TABLE II
THE PERFORMANCE OF DIFFERENT ACTIVE RANGING METHODS

Methods	Worst-case ($\max_e \{ \omega_{i,j} \}$)	RMSE $_{i,j}$
AltDS-TWR [20]	$e_{\max} d_{i,j}$	$\frac{1}{\sqrt{6}} e_{\max} d_{i,j}$
NB-TWR [27]	$e_{\max} d_{i,j}$	$\frac{1}{\sqrt{6}} e_{\max} d_{1,j}$ or $\frac{1}{3} e_{\max} d_{i,j}$ (if $i, j \neq 1$)
SM-NR	$\frac{2e_{\max}}{1+e_{\max}} d_{i,j}$	$\sqrt{\frac{8}{(N+1)(N+2)}} \frac{e_{\max} d_{i,j}}{1+e_{\max}}$

which is very similar to (32). Thus, the worst-case error and RMSE of $\hat{R}_{k;i,j}$ can be similarly derived and are provided in the following two propositions.

Proposition 6: The worst-case error of the differential range estimation $\hat{R}_{k;i,j}$ in (29) can be described as

$$\max_e \{|\omega_{k;i,j}|\} = \frac{2e_{\max}}{1+e_{\max}} |R_{k;i,j}|, \quad (35)$$

where the maximum value achieves when $e^{(n)} = -e_{\max}$ for all $n \in \mathcal{N}$.

Proposition 7: The RMSE of the differential range estimation $\hat{R}_{k;i,j}$ in (29) can be described as

$$\begin{aligned} \text{RMSE}_{k;i,j} &= \sqrt{\mathbb{E}_e \{\omega_{k;i,j}^2\}} \\ &= \sqrt{\frac{8}{(N+1)(N+2)} \frac{e_{\max} |R_{k;i,j}|}{1+e_{\max}}}. \end{aligned} \quad (36)$$

For comparison, the RMSEs of the proposed SM-NR and the popular silent ranging methods [27], [33] are summarized in Table III. From Table III we notice that, the RMSE of the TDoF estimated by the SM-NR method has the same order of magnitude as those of the existing widely-adopted silent ranging methods. While different from the existing methods, the RMSE of our work (SM-NR) is inversely proportional to N , which indicates that the accuracy of TDoF estimations will be improved by enlarging the network scale. Since silent nodes do not consume any extra time-frequency resources, it is an efficient way to improve the network ranging performance by introducing the silent working mode.

C. Effect of Timestamp Measurement Error on Ranging Precision

In this section, we evaluate the impact of timestamp measurement errors in clock model (6) on ranging precision. For ease of analyses, we consider the simplest scenario with two active nodes, and assume $e_{\max} = 0$, the measurement error $w_m^{(n)}$ is a Gaussian random variable with zero mean and variance σ_w^2 [39], and $\hat{T}^* = T^{(1)}$ without loss of generality.

Different from the clock model in (4) that the ranging performance is independent of the synchronization time T , for the clock model in (6) within the measurement error $w_m^{(n)}$, the length of synchronization time T will affect the ranging accuracy of the proposed SM-NR method. According to (6),

the ML ToF estimator of the proposed SM-NR method is given by

$$\begin{aligned} \hat{T}_{\text{oF}}(1, 2) &= \frac{1}{2} \left(\Omega_{1,2}^{(1)} - \frac{T^{(1)}}{T^{(2)}} \Omega_{1,2}^{(2)} \right) \\ &= \frac{1}{2} \left(k_1 D_{1,2}^{(1)} - \underbrace{\frac{k_1 T + w_3^{(1)} - w_1^{(1)}}{k_2 T + w_3^{(2)} - w_1^{(2)}}}_{\text{synchronization term}} (k_2 D_{1,2}^{(2)} + w_2^{(2)} - w_1^{(2)}) \right) \\ &\quad + \frac{1}{2} (w_2^{(1)} - w_1^{(1)}). \end{aligned} \quad (37)$$

It is shown that, when the synchronization time T is near 0, the synchronization term $T^{(1)}/T^{(2)}$ is approximated to $\frac{w_3^{(1)} - w_1^{(1)}}{w_3^{(2)} - w_1^{(2)}}$, while when T goes to $+\infty$, $T^{(1)}/T^{(2)}$ approximates to wanted ratio $k^{(1)}/k^{(2)}$. In other words, the effect of timestamp measurement errors will be significant when the synchronization time T is short, and slight when T is long. Thus, in practice, the interval between two signals transmitted from the first node is expected to be long in order to reduce this kind of error, i.e., $T \gg w_m^{(n)}$. Thereby, the ToF estimation (37) is approximated by

$$\begin{aligned} \hat{T}_{\text{oF}}(1, 2) &\approx \frac{1}{2} (D_{1,2}^{(1)} - D_{1,2}^{(2)}) + \frac{1}{2} (w_2^{(1)} - w_1^{(1)} - w_2^{(2)} + w_1^{(2)}) \\ &= T_{\text{oF}}(1, 2) + \frac{1}{2} (w_2^{(1)} - w_1^{(1)} - w_2^{(2)} + w_1^{(2)}). \end{aligned} \quad (38)$$

and the lower bound of the RMSE of $\hat{d}_{i,j}$ can be approximated by

$$\text{RMSE}_{1,2} = \sqrt{\mathbb{E}_w \{\omega_{1,2}^2\}} = c\sigma_w. \quad (39)$$

Remark 2: Although longer synchronization time T can reduce the impact of timestamp measurement errors on synchronization accuracy, T cannot be too large. This is because when the ranging period is long, e.g., at the second level, the assumption that the frequency deviation parameter $e^{(i)}$ is nearly fixed during the measuring period does not hold any more. In this case, the parameter $k^{(i)}/k^{(j)}$ cannot be estimated by $T^{(i)}/T^{(j)}$ and the proposed SM-NR fails. Therefore, to reduce the effect of timestamp measurement errors while maintain the usefulness of the SM-NR, we choose the interval between the first and the last signal transmissions as the synchronization time T , as shown in Fig. 3.

TABLE III
THE PERFORMANCE OF DIFFERENT SILENT RANGING METHODS

Methods	Worst-case ($\max_{\mathbf{e}} \{ \omega_{k;i,j} \}$)	RMSE $_{k;i,j}$
PER [33]	$e_{\max} \left D_{i,j}^{(k)} - \frac{T}{2} \right + e_{\max} \left D_{i,j}^{(i)} - \frac{T}{2} \right $	$\sqrt{\frac{1}{3} \left(D_{i,j}^{(k)} - \frac{T}{2} \right)^2 + \frac{1}{3} \left(D_{i,j}^{(i)} - \frac{T}{2} \right)^2} e_{\max}$
NB-PR [27]	$e_{\max} R_{k;i,j} $	$\frac{e_{\max} R_{k;1,j} }{3}$ or $\frac{e_{\max} R_{k;i,j} }{\sqrt{12}}$ (if $i, j \neq 1$)
SM-NR	$\frac{2e_{\max}}{1 + e_{\max}} R_{k;i,j} $	$\sqrt{\frac{8}{(N+1)(N+2)}} \frac{e_{\max} R_{k;i,j} }{1 + e_{\max}}$

TABLE IV
THE COMPUTATIONAL COMPLEXITIES OF DIFFERENT RANGING METHODS

Types	Methods	Computational complexities (flops)
ToF estimations	AltDS-TWR [20]	$4 \binom{N_a}{2}$
	NB-TWR [27]	$7 \binom{N_a}{2} - 3N_a + 3$
	SM-NR	$4 \binom{N_a}{2}$
TDoF estimations	PER [33]	$3N_s \binom{N_a}{2} + 3 \binom{N_a}{2}$
	NB-PR [27]	$21N_s \binom{N_a}{2} - 10N_s N_a + 10N_s$
	SM-NR	$7N_s \binom{N_a}{2}$

D. Computational Complexities of Ranging Methods

In this section, we discuss the computational complexity of the proposed SM-NR method and compare it with other ranging methods. According to (18), computing a ToF estimator requires one multiplication operation and two division operations. Then, it takes one multiplication operation to calculate the absolute range according to (29). Therefore, for a network with N_a active nodes, computing all $\binom{N_a}{2}$ absolute ranges needs $4 \binom{N_a}{2}$ flops. Similarly, according to (24), for a network with N_s silent nodes, computing all $N_s \binom{N_a}{2}$ differential ranges requires $7N_s \binom{N_a}{2}$ flops. For ease of comparison, the computational complexities of the proposed SM-NR and other popular ranging methods [20], [27], [33] are summarized in Table IV. We can observe that, the computational complexity of the proposed SM-NR has the same order of magnitude as those of the existing methods. Particularly, the complexities of all active ranging methods are $\mathcal{O}(N_a^2)$, while those of silent ranging methods are $\mathcal{O}(N_s N_a^2)$. It indicates that the computational complexity of ranging methods is proportional to the square of the network scale.

In summary, compared with existing ranging methods, the SM-NR method requires much fewer ranging signals, meanwhile higher ranging precision is achieved. Thus, we conclude that the SM-NR is an efficient and effective ranging method for networks under clock effects. To further demonstrate the conclusion, numerical comparisons are provided in Section VI.

V. NETWORK LOCALIZATION FOR ACTIVE AND SILENT NODES

In this section, we will show how to realize network localization using the obtained absolute and differential range measurements for both active and silent nodes, and evaluate its performance under a relative coordinate transformation metric for arbitrary translation and rotation.

A. Joint Network Localization Algorithm

Based on the least square criteria, the node position \mathbf{p} in (1) is jointly estimated by minimizing the cost function $L(\mathbf{p})$, which is formulated as

$$L(\mathbf{p}) = \frac{2}{N_a(N_a - 1)} \sum_{i,j \in N_a} \eta_{i,j} f_{i,j}(\mathbf{p}) + \frac{2}{N_a(N_a - 1)N_s} \sum_{i,j \in N_a} \sum_{k \in N_s} \eta_{k;i,j} g_{k;i,j}(\mathbf{p}) \quad (40)$$

where $\sum_{i,j \in N_a} := \sum_{i=1}^{N_a} \sum_{j=i+1}^{N_a}$, $\eta_{i,j}$ and $\eta_{k;i,j}$ are the confidences of absolute estimation and differential range estimation, given by

$$\eta_{i,j} = \frac{1}{\sqrt{\text{Var}_{\mathbf{e}}\{\omega_{i,j}\}}} \quad \text{and} \quad \eta_{k;i,j} = \frac{1}{\sqrt{\text{Var}_{\mathbf{e}}\{\omega_{k;i,j}\}}}$$

and $f_{i,j}(\mathbf{p})$ and $g_{k;i,j}(\mathbf{p})$ are the square errors of $\hat{d}_{i,j}$ and $\hat{R}_{k;i,j}$, i.e.,

$$f_{i,j}(\mathbf{p}) = \left(\|\mathbf{p}_i - \mathbf{p}_j\| - \hat{d}_{i,j} \right)^2$$

$$g_{k;i,j}(\mathbf{p}) = \left(\|\mathbf{p}_i - \mathbf{p}_k\| - \|\mathbf{p}_j - \mathbf{p}_k\| - \hat{R}_{k;i,j} \right)^2.$$

The Newton's method is adopted to minimize $L(\mathbf{p})$ and the iterative scheme is given by

$$\hat{\mathbf{p}}^{(r+1)} = \hat{\mathbf{p}}^{(r)} - \zeta^{(r)} \mathbf{v}^{(r)} \quad (41)$$

where $\mathbf{v}^{(r)}$ is the r -th iteration direction, i.e.,

$$\mathbf{v}^{(r)} = \left. \frac{\partial L(\mathbf{p})}{\partial \mathbf{p}} \right|_{\mathbf{p}=\hat{\mathbf{p}}^{(r)}} \quad (42)$$

and the step length $\zeta^{(r)}$ is determined as

$$\zeta^{(r)} = \frac{\|\mathbf{v}^{(r)}\|^2}{(\mathbf{v}^{(r)})^T \mathbf{H}^{(r)} \mathbf{v}^{(r)}} \quad (43)$$

in which $\mathbf{H}^{(r)} \in \mathbb{R}^{2N \times 2N}$ is the Hessian matrix of $L(\mathbf{p})$, i.e.,

$$[\mathbf{H}^{(r)}]_{i,j} = \left. \frac{\partial^2 L(\mathbf{p})}{\partial [p]_i \partial [p]_j} \right|_{\mathbf{p}=\hat{\mathbf{p}}^{(r)}}.$$

Since the cost function $L(\mathbf{p})$ is non-convex, the optimization result highly depends on the selection of initial point. To improve the accuracy, the positions of active nodes are initialized using the multidimensional scaling (MDS) relative localization method [48] and the positions of silent nodes are initialized by the MDS-based time-difference-of-arrival (TDOA) method [49]. The proposed joint network localization algorithm is summarized in Algorithm 2.

B. Relative Position Transformation

In general, the position estimations $\hat{\mathbf{p}}$ from Algorithm 2 may be much different from the true positions \mathbf{p} , since the network lacks absolute coordinate reference. Indeed, the position estimations $\hat{\mathbf{p}}$ from Algorithm 2 only characterize the relative geometric relationships among nodes, i.e., the shape of the network [50]. Thus, to better evaluate the performance of Algorithm 2, we turn to the relative coordinate paradigm, in which two shapes that are interconvertible through translation, rotation and reflecting are viewed as the same one. The detailed definition regarding relative localization is given as follows.

Given an estimation $\hat{\mathbf{p}}$, the relative position transformation of $\hat{\mathbf{p}}$ is given by [51], [52]

$$S_{\Psi}(\hat{\mathbf{p}}) = \mathbf{R}_{\Psi} \hat{\mathbf{p}} + [\lambda_x \ \lambda_y] \boldsymbol{\nu} \quad (44)$$

where $\mathbf{R}_{\Psi} = \text{diag}\{\Gamma_{\varphi}, \Gamma_{\varphi}, \dots, \Gamma_{\varphi}\} \in \mathbb{R}^{2N \times 2N}$ with $\Gamma_{\varphi} \in \mathbb{R}^{2 \times 2}$ being the rotation matrices and taking the form of

$$\Gamma_{\varphi} = \begin{bmatrix} \cos \varphi & -\sin \varphi \\ \sin \varphi & \cos \varphi \end{bmatrix} \quad (45)$$

in which φ is the rotating angles of the topology. The notation $\boldsymbol{\nu} = [\Delta x \ \Delta y]^T \in \mathbb{R}^2$ is the translation vector, and

$$\begin{aligned} \lambda_x &= [1, 0, 1, 0, \dots, 1, 0]^T \in \mathbb{R}^{2N} \\ \lambda_y &= [0, 1, 0, 1, \dots, 0, 1]^T \in \mathbb{R}^{2N} \end{aligned} \quad (46)$$

Then, the transformation vector is defined as $\Psi = [\varphi \ \boldsymbol{\nu}]^T$.

Algorithm 2 Network Localization for Active and Silent Nodes

Input: ToF estimations $\hat{\mathbf{T}}_{\text{oF}}(i, j)$ and TDoF estimations $\hat{\mathbf{T}}_{\text{d}}(k; i, j)$ ($i, j \in \mathcal{N}_{\text{a}}, k \in \mathcal{N}_{\text{s}}$).

Output: Node position estimations $\hat{\mathbf{p}}$.

- 1: Calculate absolute/differential distances according to (29);
 - 2: Initialize all active node positions by the MDS localization method [48];
 - 3: Initialize all silent node positions by the MDS-based TDOA method [49];
 - 4: $r \leftarrow 0$;
 - 5: **while** no convergence of cost function $L(\hat{\mathbf{p}}^{(r)})$ **do**
 - 6: Calculate the iteration direction $\mathbf{v}^{(r)}$ and the step length $\zeta^{(r)}$ by (42) and (43), respectively;
 - 7: Update the positions $\hat{\mathbf{p}}^{(r)}$;
 - 8: Calculate the cost function $L(\hat{\mathbf{p}}^{(r)})$ by (40);
 - 9: $r \leftarrow r + 1$;
 - 10: **end while**
 - 11: **return** Position estimations $\hat{\mathbf{p}}$.
-

We aim to find the optimal transformation parameter Ψ which minimizes the difference between $\hat{\mathbf{p}}$ and \mathbf{p} by neglecting translation, rotation, and reflecting errors, i.e.,

$$\Psi^* = \underset{\Psi}{\text{argmin}} \|\mathbf{S}_{\Psi}(\hat{\mathbf{p}}) - \mathbf{p}\|^2. \quad (47)$$

The optimal solution to the above optimization problem (47) has been given in [53], given by

$$\begin{aligned} \Gamma_{\varphi}^* &= \mathbf{V} \mathbf{U}^T \\ \mathbf{v}^* &= \left(\mathbf{M}^T - \Gamma_{\varphi}^* \hat{\mathbf{M}}^T \right) \mathbf{1}_N / N \end{aligned} \quad (48)$$

where $\hat{\mathbf{M}} = [\hat{\mathbf{p}}_1, \dots, \hat{\mathbf{p}}_N]^T \in \mathbb{R}^{N \times 2}$, $\mathbf{M} = [\mathbf{p}_1, \dots, \mathbf{p}_N]^T \in \mathbb{R}^{N \times 2}$, and matrix $\mathbf{U} \mathbf{L} \mathbf{V}^T$ is the singular value decomposition of $\hat{\mathbf{M}}^T (I - N^{-1} \mathbf{1}_N \mathbf{1}_N^T) \mathbf{M}$. With optimal Ψ^* , the optimal position estimation $\hat{\mathbf{p}}$ after relative transformation is given by

$$\hat{\mathbf{p}}_{\text{opt}} = \mathbf{S}_{\Psi^*}(\hat{\mathbf{p}}). \quad (49)$$

Finally, the averaged relative position error for the whole network is defined as

$$\varepsilon = \sqrt{\frac{\|\hat{\mathbf{p}}_{\text{opt}} - \mathbf{p}\|^2}{N}}. \quad (50)$$

VI. NUMERICAL SIMULATION RESULTS

A. Benchmarks and Setups

In this section, we evaluate the effectiveness and efficiency of the proposed SM-NR method and the network localization algorithm with following 4 benchmarks:

- **Benchmark 1** (AltDS-TWR [20]): A popular active ranging method [30], which measures one absolute range using three ranging signals.
- **Benchmark 2** (PER [33]): A popular silent ranging method, which can measure a differential range without extra ranging signal required. Note that the PER works associated with the active ranging method AltDS-TWR [33].

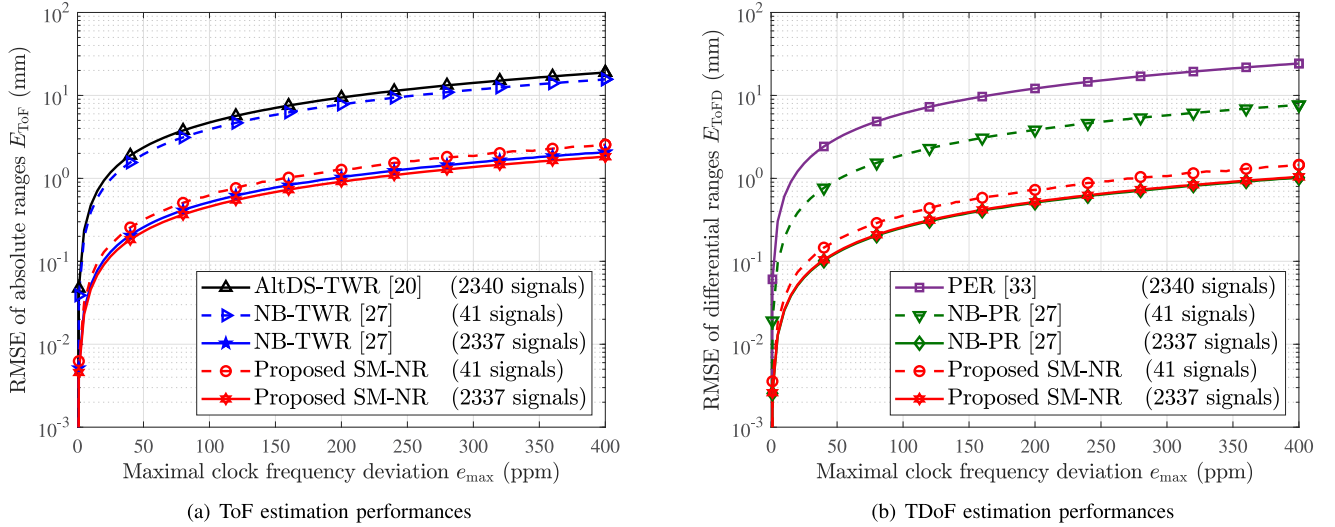


Fig. 4. The RMSE of (a) absolute ranges; (b) differential ranges against the maximal clock frequency deviation e_{\max} .

- **Benchmark 3** (NB-TWR [27]): An active ranging method in a parallel work of ours [27], which can measure all absolute ranges in the network simultaneously and requires the same number of ranging signals as the proposed SM-NR.
- **Benchmark 4** (NB-PR [27]): A silent ranging method in a parallel work of ours [27], which can measure all differential ranges without extra signal overhead. Note that the NB-PR only works with the active ranging method NB-TWR.

We consider a 2-D scenario with N_a active nodes and N_s silent nodes being randomly distributed in a $200\text{m} \times 200\text{m}$ square plane. The response delays of all nodes are set as 1 ms. The clock frequency deviations for all nodes $e^{(n)}$ $n \in \mathcal{N}$ is modeled as uniformly random variables bounded by $[-e_{\max}, +e_{\max}]$ [21], [30], [39]. All the simulation results in figures are the average results of 10000 independent experiments, and the adopted performance metric to evaluate the estimation performance is the average RMSE of $\binom{N_a}{2}$ absolute ranges or $N_s \binom{N_a}{2}$ differential ranges, i.e.,

$$E_{\text{ToF}} = \mathbb{E} \left\{ \sqrt{\frac{2}{N_a(N_a-1)} \sum_{i,j \in \mathcal{N}_a} \omega_{i,j}^2} \right\}$$

$$E_{\text{TDoF}} = \mathbb{E} \left\{ \sqrt{\frac{2}{N_s N_a(N_a-1)} \sum_{i,j \in \mathcal{N}_a} \sum_{k \in \mathcal{N}_s} \omega_{k;i,j}^2} \right\} \quad (51)$$

where $\omega_{i,j}$ and $\omega_{k;i,j}$ are defined in (32) and (34), respectively.

B. RMSE of the SM-NR

We first evaluate the performance of the proposed SM-NR method under the ideal clock model in (4), where only the clock drifts affect the accuracy of timestamp measurements. This ideal case can serve as a performance limit for systems which will be influenced by other clock factors.

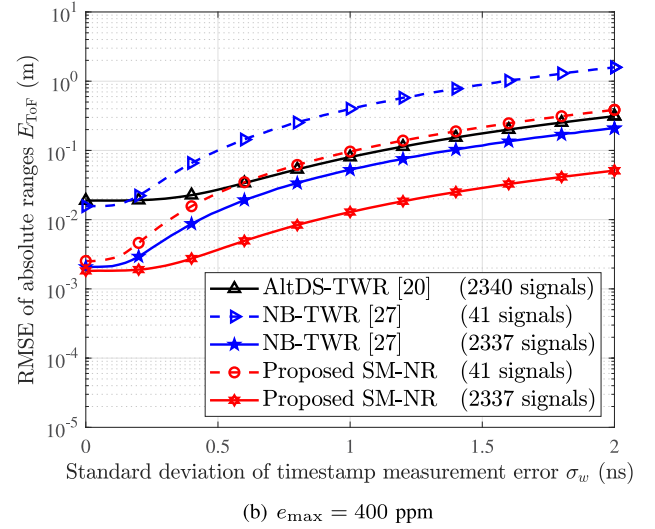
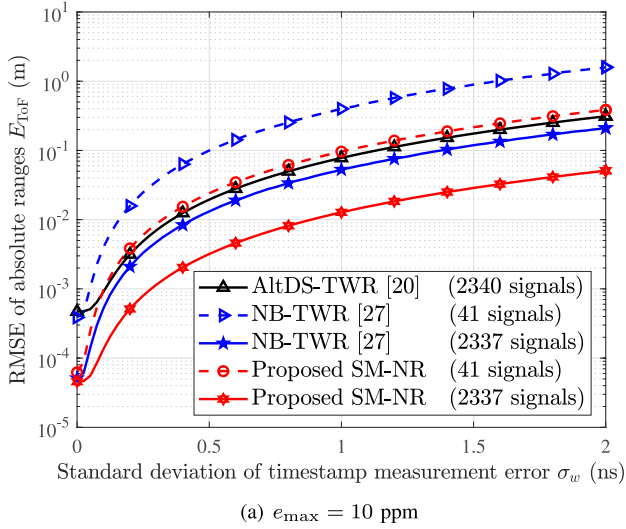
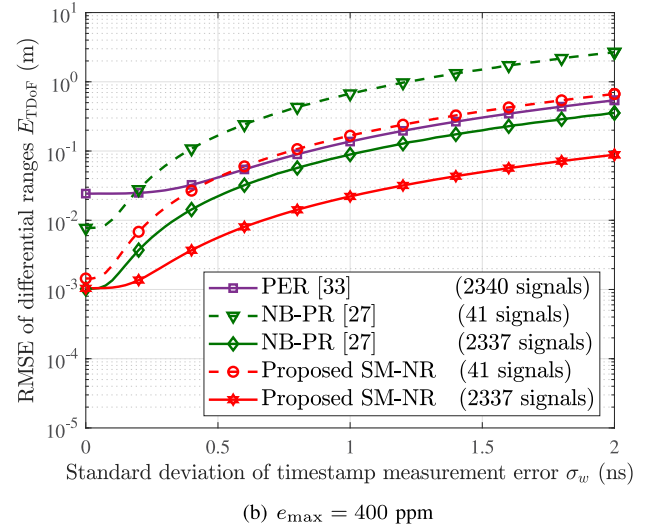
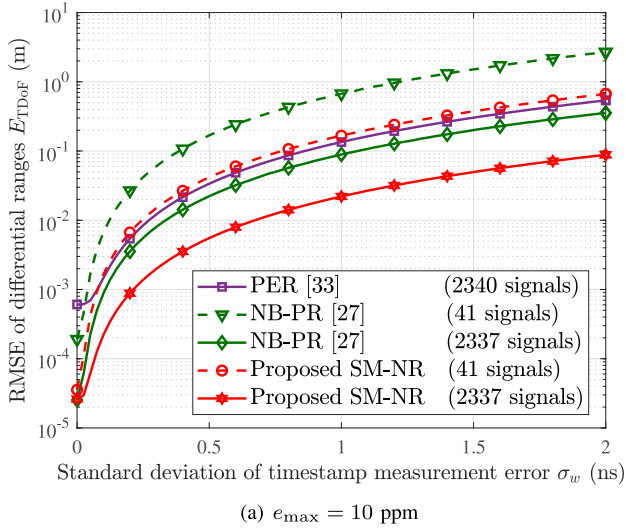
Let $N_a = 40$ and $N_s = 10$. To measure all 780 absolute ranges and 7800 differential ranges in the network, it requires

2340 signals for AltDS-TWR [20], while only 41 signals are required by NB-TWR [27] and the proposed SM-NR method. For fair comparisons, in each experiment, the total consumed signals are constrained as 2340. Subject to this constraint, NB-TWR and the proposed SM-NR are performed $\lfloor 2340/41 \rfloor = 57$ times and consume 2337 signals in total. Then, 57 output results of NB-TWR and SM-NR are averaged as their range measurements.

By jointly performing active and silent ranging methods, we plot the RMSEs of absolute ranges and differential ranges against the maximal clock frequency deviation e_{\max} in Fig. 4 (a) and Fig. 4 (b), respectively. From the two figures, we have the following three observations. First, the RMSE of the proposed SM-NR are at the millimeter order, indicating it successfully eliminates most of the errors caused by clock drifts, as discussed in Section IV. Second, as the clock drift effect becomes more significant, i.e., e_{\max} becomes larger, the RMSEs of all these three methods increase. Nevertheless, the RMSE of the proposed SM-NR method is about one order of magnitude lower than those of the other methods. For example, for the ToF estimations, when e_{\max} is 200 ppm with 2337 signals, the RMSE of the SM-NR is about 0.9 mm, while those of NB-TWR and AltDS-TWR are 1.1 mm and 9.4 mm, respectively. As for the silent ranging, the RMSE of the proposed SM-NR method is about 0.51 mm, while those of NB-PR and PER are 0.52 mm and 12.1 mm, respectively. Moreover, even when SM-NR is only performed once which consumes 41 signals, the RMSE of SM-NR is still much smaller than those of the traditional methods, which reveals the robustness of the SM-NR against the effect of clock drifts. To sum up, these results show the superior performance of the SM-NR in the presence of clock drifts.

C. RMSE of SM-NR in the Presence of Timestamp Measurement Errors

In this section, we evaluate the performance of the proposed SM-NR method under the effect of timestamp measurement


 Fig. 5. The RMSE of absolute ranges against the standard deviation of timestamp measurement error σ_w .

 Fig. 6. The RMSE of differential ranges against the standard deviation of timestamp measurement error σ_w .

error w with the clock model (6). Similar to [17], [39], here we assume the measurement errors of timestamps $w_m^{(n)}$ are Gaussian distributed with zero mean and variance σ_w^2 . We fix the maximal clock frequency deviation e_{\max} as 10 ppm and 400 ppm, and the other system settings are similar as the previous section.

The RMSEs of absolute ranges and differential ranges as functions of the standard deviation of timestamp measurement error σ_w are shown in Fig. 5 and Fig. 6, respectively. There are three observations worth noting. First, for ToF and TDoF estimations, with different e_{\max} , the RMSEs grow from different initial values. For example, the lowest RMSE of AltDS-TWR is 0.47 mm when $e_{\max} = 10$ ppm and becomes 18.9 mm when $e_{\max} = 400$ ppm. The reason is that, when the timestamp measurement error is low, the factors causing range estimation errors are dominated by the clock drifts. In contrast, when $\sigma_w > 1$ ns, the differences between the two cases with different e_{\max} disappear. It is because the factors causing ranging errors are dominated by the clock measurement errors when σ_w is large enough. Second, we observe that the RMSE of the SM-NR method is one order of magnitude lower than those of

other existing methods. For example, when $e_{\max} = 10$ ppm and $\sigma_w = 2$ ns, for the ToF estimations shown in Fig. 5, the RMSEs of AltDS-TWR, NB-TWR, and the proposed SM-NR method are 31 cm, 21 cm, and 5.1 cm, respectively. While for silent ranging, as shown in Fig. 5, the RMSEs of PER, NB-PR, and the proposed SM-NR method are 53 cm, 35 cm, and 8.8 cm, respectively. This result indicates that, constrained by the consumed signals in total, the proposed joint synchronization and ranging methods are much more robust against the timestamp measurement errors. Finally, we also note that, when all methods are only performed once, the RMSE of NB-TWR and PER are about an order of magnitude higher than those of the other methods. The reason is that the synchronization time of NB-TWR is very short, which is determined by its inherent ranging protocol [27]. As we have discussed in Section IV-C, shorter synchronization time will amplify the effect of timestamp measurement error on clock synchronization, which leads to larger ranging error. Consequently, we can conclude that, our proposed SM-NR method will provide a much more robust ranging service for high-precision network localization.

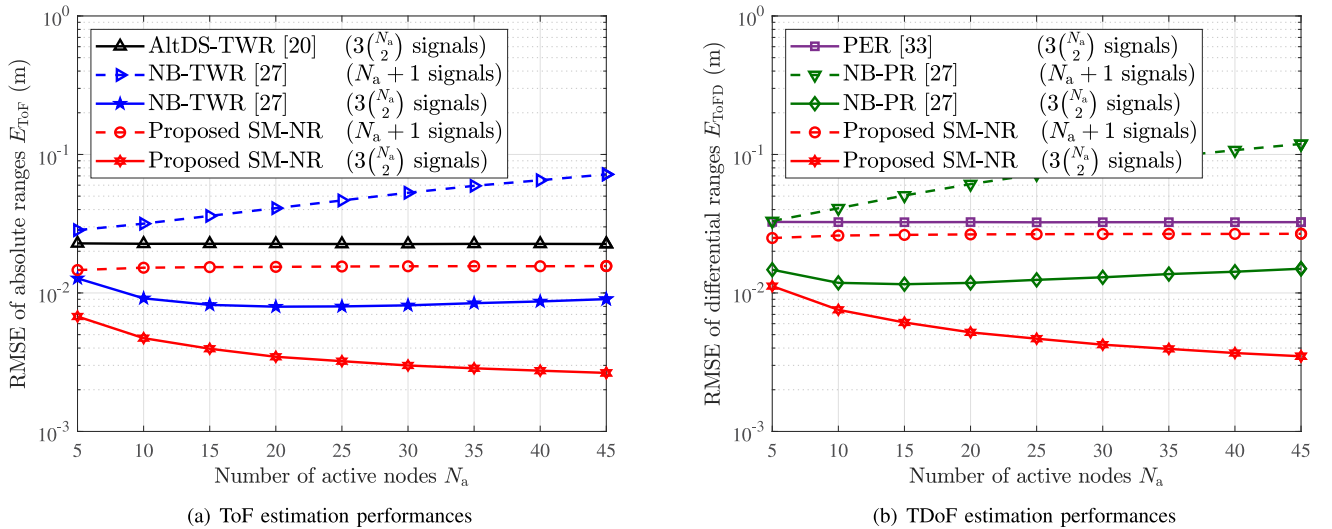


Fig. 7. The RMSE of (a) absolute ranges (b) differential ranges against the maximal clock frequency deviation e_{\max} .

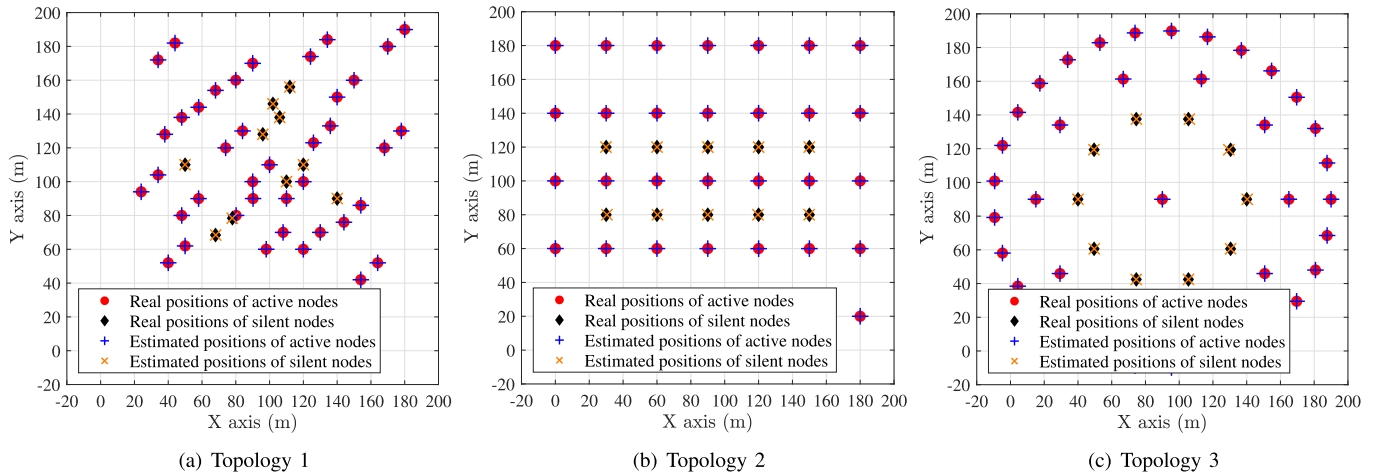


Fig. 8. Three different topologies of networks with 40 active nodes and 10 silent nodes. The position estimation results are obtained from the combination of Algorithm 1, Algorithm 2, and the relative position transformation in Section V-B.

D. RMSE of the SM-NR With Different Ratios of Active Nodes to Silent Nodes

To evaluate the effect of the ratio of active nodes to silent nodes on ranging accuracy, here we fix the total number of network nodes as $N_a + N_s = 50$, and then we set $e_{\max} = 400$ ppm and $\sigma_w = 0.4$ ns. The RMSE of different ranging methods as a function of the number of active nodes N_a is shown in Fig. 7.

From these two figures, we observe that the accuracies of AltDS-TWR and PER are almost unchanged with the increasing number of active nodes N_a . This is because these two methods adopt the node-to-node ranging protocol and thus do not depend on the number of active nodes. Besides, the accuracy of NB-TWR and NB-PR become worse as the number of active nodes increases. It is for the reason that, as the number of active nodes N_a increases, the total consumed time of the ranging protocol of NB-TWR and NB-PR becomes longer. Since the synchronization time of NB-TWR and NB-PR is fixed, the synchronization time becomes relatively shorter compared with the total ranging time, and thus the influence of timestamp measurement error on ranging is gradually amplified, as discussed in Section IV-C. By contrast, we can observe

that the proposed SM-NR method keeps a good performance in both active and silent ranging. Particularly, its accuracy becomes higher as N_a increases. The reasons are two-fold. Firstly, the synchronization time T in SM-NR becomes longer, which alleviates the effect of timestamp measurement error on ranging accuracy, as discussed in Section IV-C. Secondly, more active nodes in the network means that, more wideband signals are utilized for ranging, which brings more timestamp observations thus improving the accuracy.

E. RMSE of Proposed Network Localization Algorithm

Next, we analyze the performance of the proposed network localization algorithm. As discussed in Section IV, the accuracies of the ranging methods are influenced by the ranges, while the localization accuracy critically depends on the ranging accuracy. We consider one random topology and two typical network topologies in Fig. 8, where the maximal clock frequency deviation is $e_{\max} = 400$ ppm, the standard deviation of timestamp measurement error is $\sigma_w = 2$ ns, and the estimated positions of active and silent nodes are determined by performing the proposed SM-NR method. From Fig. 8, we observe that the positions of all active nodes and

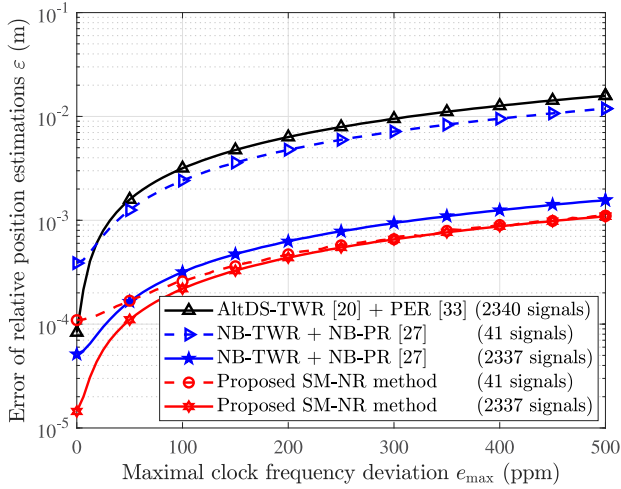


Fig. 9. The error of relative position estimations ε against the maximal clock frequency deviation e_{\max} where $\sigma_w = 50$ ps.

silent nodes are precisely estimated, with errors no larger than 10 cm, which demonstrates the effectiveness of the proposed SM-NR method and the network localization algorithm.

We adopt the randomly generated topology in Fig. 8 (a) for further evaluations. The relative position errors against the maximal clock frequency deviation e_{\max} and the clock measurement error σ_w are presented in Fig. 9 and Fig. 10, respectively, where the performance metric, the relative position error ε , is defined in (50). First, we observe that the overall trends of relative localization errors are consistent with those of the ranging errors, and the relative localization errors of the proposed SM-NR method are about one order of magnitude lower than those of the other methods. For example, when the clock measurement error is $\sigma_w = 2$ ns, the errors of AltDS-TWR+PER, NB-TWR+NB-PR, and the proposed SM-NR are 13.3 cm, 8.3 cm, and 2.3 cm, respectively, which meets the requirement of high-precision localization. Second, since both of the timestamp measurement error and the clock drift error will affect the localization performance, appropriate ways should be adopted case by case to mitigate the position estimation error in practical systems. For example, from Fig. 9, we note that when the clock measurement error is small (i.e. $\sigma_w = 50$ ps), the clock drifts dominate and thus the localization performance can be greatly improved by employing more stable clocks. In contrast, when the clock frequency deviation is small (i.e. $e_{\max} = 10$ ppm), the timestamp measurement error dominates and then improving the signal transmit power and sampling rate, will be more efficient in improving the localization accuracy.

VII. CONCLUSION

In this paper, we established a high-efficiency localization framework, which fully mitigates the clock drifts using a minimum number of transmissions. Specifically, a network ranging method named SM-NR was proposed, which consists of a ranging protocol with the minimum required number of signal transmissions, and an ML range estimator which effectively mitigates clock drifts. Then, with the range estimations, the positions of active and silent nodes can

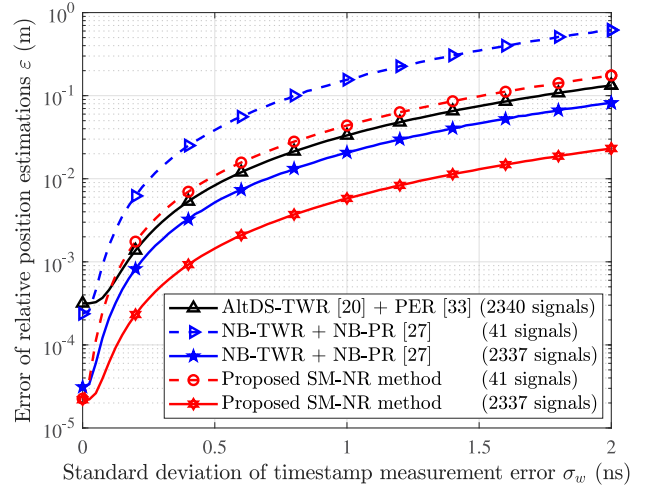


Fig. 10. The error of relative position estimations ε against the standard deviation of timestamp measurement error σ_w , where $e_{\max} = 10$ ppm.

be jointly determined. Performance analysis and simulation results showed that compared with the state-of-the-art ranging methods, the proposed SM-NR can achieve orders of magnitude accuracy enhancement with much lower signal overhead. This work provides a guideline to achieve high-precision network localization under the influences of clock drifts with low signal overhead, especially for large-scale networks.

For follow-up works, several issues are worth further investigations. First, this paper mainly focuses on centralized networks, and designing efficient distributed ranging and localization schemes needs further investigations. Second, the operating mode and the scheduling strategy are assumed known in this paper. Determining which nodes forward data, optimizing the scheduling strategy, and designing an Ad hoc ranging network are also important issues. Moreover, extensions of the proposed method allowing the inclusion of non-ideal wireless propagation such as multipath effects are of interest.

APPENDIX A PROOF OF PROPOSITION 5

According to (34), the RMSE of $d_{i,j}$ can be rewritten as

$$\begin{aligned} \text{RMSE}_{i,j} &= \sqrt{\mathbb{E}_{\mathbf{e}}\{\omega_{i,j}^2\}} \\ &= \sqrt{\frac{\mathbb{E}_{\mathbf{e}}\{Y^2\}}{T^2(1+e_{\max})^2} + 1 - 2\frac{\mathbb{E}_{\mathbf{e}}\{Y\}}{T(1+e_{\max})}} d_{i,j} \end{aligned} \quad (52)$$

where $Y := \max_{n \in \mathcal{N}} \{T^{(n)}\}$. Since $\mathbf{e}^{(n)}$ is uniformly distributed in $[-e_{\max}, +e_{\max}]$, each $T^{(n)}$ is uniformly distributed in the range $[(1-e_{\max})T, (1+e_{\max})T]$, and thus the cumulative distribution function (CDF) of Y can be written as

$$F_Y(y) = \begin{cases} \prod_{n=1}^N \frac{y - (1-e_{\max})T}{2e_{\max}T}, & -e_{\max} \leq \frac{y}{T} - 1 \leq e_{\max}, \\ 0, & \text{otherwise.} \end{cases} \quad (53)$$

$$\begin{aligned}
\text{RMSE}_{i,j} &= \sqrt{\frac{\frac{4Ne_{\max}^2}{N+2} + (1 - e_{\max})^2 + \frac{4N(1-e_{\max})e_{\max}}{N+1}}{(1 + e_{\max})^2} + 1 - \frac{\frac{4Ne_{\max}}{N+1} + 2(1 - e_{\max})}{(1 + e_{\max})}} d_{i,j} \\
&= \sqrt{\frac{\frac{4Ne_{\max}^2}{N+2} - \frac{8Ne_{\max}^2}{N+1} + 4e_{\max}^2}{(1 + e_{\max})^2}} d_{i,j} = \sqrt{\frac{8}{(N + 2)(N + 1)}} \frac{e_{\max} d_{i,j}}{(1 + e_{\max})}. \tag{57}
\end{aligned}$$

Then, the PDF of Y can be derived as

$$f_Y(y) = \begin{cases} \frac{N}{(2e_{\max}T)^N} (y - (1 - e_{\max})T)^{N-1}, & -e_{\max} \leq \frac{y}{T} - 1 \leq e_{\max}, \\ 0, & \text{otherwise.} \end{cases} \tag{54}$$

With the PDF of Y , the expectations of Y and Y^2 can be calculated as

$$\begin{aligned}
\mathbb{E}_e \{Y\} &= \frac{N}{(2e_{\max}T)^N} \\
&\quad \times \int_{(1-e_{\max})T}^{(1+e_{\max})T} y(y - (1 - e_{\max})T)^{N-1} dy \\
&= \frac{N}{(2e_{\max}T)^N} \int_0^{2e_{\max}T} z^N dz \\
&\quad + \frac{N(1 - e_{\max})T}{(2e_{\max}T)^N} \int_0^{2e_{\max}T} z^{N-1} dz \\
&= \frac{2Ne_{\max}T}{N+1} + (1 - e_{\max})T \tag{55}
\end{aligned}$$

$$\begin{aligned}
\mathbb{E}_e \{Y^2\} &= \frac{N}{(2e_{\max}T)^N} \\
&\quad \times \int_{(1-e_{\max})T}^{(1+e_{\max})T} y^2(y - (1 - e_{\max})T)^{N-1} dy \\
&= \frac{N}{(2e_{\max}T)^N} \int_0^{2e_{\max}T} z^{N+1} dz \\
&\quad + \frac{N(1 - e_{\max})^2 T^2}{(2e_{\max}T)^N} \int_0^{2e_{\max}T} z^{N-1} dz \\
&\quad + \frac{2(1 - e_{\max})TN}{(2e_{\max}T)^N} \int_0^{2e_{\max}T} z^N dz \\
&= \frac{4Ne_{\max}^2 T^2}{N+2} + (1 - e_{\max})^2 T^2 \\
&\quad + \frac{4N(1 - e_{\max})e_{\max} T^2}{N+1}. \tag{56}
\end{aligned}$$

By substituting (55) and (56) into (52), we obtain the closed-form of $\text{RMSE}_{i,j}$ (57) as shown at the top of the page, which completes the proof.

REFERENCES

- [1] M. Z. Win, Y. Shen, and W. Dai, "A theoretical foundation of network localization and navigation," *Proc. IEEE*, vol. 106, no. 7, pp. 1136–1165, Jul. 2018.
- [2] N. M. Freris, H. Kowshik, and P. R. Kumar, "Fundamentals of large sensor networks: Connectivity, capacity, clocks, and computation," *Proc. IEEE*, vol. 98, no. 11, pp. 1828–1846, Nov. 2010.
- [3] B. Wang, Q. Xu, C. Chen, F. Zhang, and K. R. Liu, "The promise of radio analytics: A future paradigm of wireless positioning, tracking, and sensing," *IEEE Signal Process. Mag.*, vol. 35, no. 3, pp. 59–80, May 2018.
- [4] Y. Wang, K. Gu, Y. Wu, W. Dai, and Y. Shen, "NLOS effect mitigation via spatial geometry exploitation in cooperative localization," *IEEE Trans. Wireless Commun.*, vol. 19, no. 9, pp. 6037–6049, Sep. 2020.
- [5] A. Conti, M. Guerra, D. Dardari, N. Decarli, and M. Z. Win, "Network experimentation for cooperative localization," *IEEE J. Sel. Areas Commun.*, vol. 30, no. 2, pp. 467–475, Feb. 2012.
- [6] S. Mazuelas, A. Conti, J. C. Allen, and M. Z. Win, "Soft range information for network localization," *IEEE Trans. Signal Process.*, vol. 66, no. 12, pp. 3155–3168, Jun. 2018.
- [7] S. Bartoletti, A. Conti, W. Dai, and M. Z. Win, "Threshold profiling for wideband ranging," *IEEE Signal Process. Lett.*, vol. 25, no. 6, pp. 873–877, Jun. 2018.
- [8] S. Bartoletti, W. Dai, A. Conti, and M. Z. Win, "A mathematical model for wideband ranging," *IEEE J. Sel. Topics Signal Process.*, vol. 9, no. 2, pp. 216–228, Mar. 2015.
- [9] D. Jourdan, D. Dardari, and M. Win, "Position error bound for UWB localization in dense cluttered environments," *IEEE Trans. Aerosp. Electron. Syst.*, vol. 44, no. 2, pp. 613–628, Apr. 2008.
- [10] K.-L. Noh, E. Serpedin, and K. Qaraqe, "A new approach for time synchronization in wireless sensor networks: Pairwise broadcast synchronization," *IEEE Trans. Wireless Commun.*, vol. 7, no. 9, pp. 3318–3322, Sep. 2008.
- [11] M. Ouellette, K. Ji, S. Liu, and H. Li, "Using IEEE 1588 and boundary clocks for clock synchronization in telecom networks," *IEEE Commun. Mag.*, vol. 49, no. 2, pp. 164–171, Feb. 2011.
- [12] Y. Liu, Y. Shen, D. Guo, and M. Z. Win, "Network localization and synchronization using full-duplex radios," *IEEE Trans. Signal Process.*, vol. 66, no. 3, pp. 714–728, Feb. 2018.
- [13] Y.-C. Wu, Q. Chaudhari, and E. Serpedin, "Clock synchronization of wireless sensor networks," *IEEE Signal Process. Mag.*, vol. 28, no. 1, pp. 124–138, Jan. 2011.
- [14] F. Lamonaca, A. Gasparri, E. Garone, and D. Grimaldi, "Clock synchronization in wireless sensor network with selective convergence rate for event driven measurement applications," *IEEE Trans. Instrum. Meas.*, vol. 63, no. 9, pp. 2279–2287, Sep. 2014.
- [15] Y. Xiong, N. Wu, Y. Shen, and M. Z. Win, "Cooperative network synchronization: Asymptotic analysis," *IEEE Trans. Signal Process.*, vol. 66, no. 3, pp. 757–772, Feb. 2018.
- [16] Q. Tian, D.-Z. Feng, H.-S. Hu, F. Yang, and L. Wei, "Bi-iterative algorithm for joint localization and time synchronization in wireless sensor networks," *Signal Process.*, vol. 154, pp. 304–313, Jan. 2019.
- [17] Y. Wang, X. Ma, and G. Leus, "Robust time-based localization for asynchronous networks," *IEEE Trans. Signal Process.*, vol. 59, no. 9, pp. 4397–4410, Sep. 2011.
- [18] T. Wang, H. Zhao, and Y. Shen, "An efficient single-anchor localization method using ultra-wide bandwidth systems," *Appl. Sci.*, vol. 10, no. 1, p. 57, Dec. 2019.
- [19] P. Ferrari *et al.*, "Timestamping and ranging performance for IEEE 802.15.4 CSS systems," *IEEE Trans. Instrum. Meas.*, vol. 63, no. 5, pp. 1244–1252, May 2014.
- [20] D. Neiryck, E. Luk, and M. McLaughlin, "An alternative double-sided two-way ranging method," in *Proc. 13th Workshop Positioning, Navigat. Commun. (WPNC)*, Banff, AB, Canada, Oct. 2016, pp. 1–4.
- [21] C. L. Sang, M. Adams, T. Hörmann, M. Hesse, M. Pörmann, and U. Rückert, "An analytical study of time of flight error estimation in two-way ranging methods," in *Proc. Int. Conf. Indoor Positioning Indoor Navigat. (IPIN)*, Nantes, France, Sep. 2018, pp. 1–8.
- [22] M. Kwak and J. Chong, "A new double two-way ranging algorithm for ranging system," in *Proc. 2nd IEEE Int. Conf. Netw. Infrastruct. Digit. Content*, Beijing, China, Sep. 2010, pp. 470–473.
- [23] H. Kim, "Double-sided two-way ranging algorithm to reduce ranging time," *IEEE Commun. Lett.*, vol. 13, no. 7, pp. 486–488, Jul. 2009.

- [24] Y. Jiang and V. C. M. Leung, "An asymmetric double sided two-way ranging for crystal offset," in *Proc. Int. Symp. Signals, Syst. Electron.*, Montreal, QC, Canada, Jul. 2007, pp. 525–528.
- [25] D. Oh, M. Kwak, and J.-W. Chong, "A subspace-based two-way ranging system using a chirp spread spectrum modem, robust to frequency offset," *IEEE Trans. Wireless Commun.*, vol. 11, no. 4, pp. 1478–1487, Apr. 2012.
- [26] J. X. Lee, Z. W. Lin, P. S. Chin, and C. L. Law, "The use of symmetric multi-way two phase ranging to compensate time drift in wireless sensor network," *IEEE Trans. Wireless Commun.*, vol. 8, no. 2, pp. 613–616, Feb. 2009.
- [27] Z. Zhang, H. Zhao, and Y. Shen, "High-efficient ranging algorithms for wireless sensor network," in *Proc. 11th Int. Conf. Wireless Commun. Signal Process. (WCSP)*, Xi'an, China, Oct. 2019, pp. 1–6.
- [28] R. Dalce, A. van den Bossche, and T. Val, "An experimental performance study of an original ranging protocol based on an IEEE 802.15.4a UWB testbed," in *Proc. IEEE Int. Conf. Ultra-WideBand (ICUWB)*, Paris, France, Sep. 2014, pp. 7–12.
- [29] R. Dalce, A. van den Bossche, and T. Val, "A study of the ranging error for parallel double sided-two way ranging protocol," in *Proc. IEEE 84th Veh. Technol. Conf. (VTC-Fall)*, Montreal, QC, Canada, Sep. 2016, pp. 1–5.
- [30] C. L. Sang, M. Adams, T. Hörmann, M. Hesse, M. Pormann, and U. Rückert, "Numerical and experimental evaluation of error estimation for two-way ranging methods," *Sensors*, vol. 19, no. 3, p. 616, Feb. 2019.
- [31] M. Pelka and H. Hellbrück, "S-TDoA—Sequential time difference of arrival—A scalable and synchronization free approach for positioning," in *Proc. IEEE Wireless Commun. Netw. Conf.*, Doha, Qatar, Apr. 2016, pp. 1–6.
- [32] K. A. Horváth, G. Ill, and Á. Milánkovich, "Passive extended double-sided two-way ranging algorithm for UWB positioning," in *Proc. 9th Int. Conf. Ubiquitous Future Netw. (ICUFN)*, Milan, Italy, Jul. 2017, pp. 482–487.
- [33] K. A. Horváth, G. Ill, and Á. Milánkovich, "Passive extended double-sided two-way ranging with alternative calculation," in *Proc. IEEE 17th Int. Conf. Ubiquitous Wireless Broadband (ICUWB)*, Salamanca, Italy, Sep. 2017, pp. 1–5.
- [34] Y. Han *et al.*, "Performance limits and geometric properties of array localization," *IEEE Trans. Inf. Theory*, vol. 62, no. 2, pp. 1054–1075, Feb. 2016.
- [35] H. Zhao, N. Zhang, and Y. Shen, "Beamspace direct localization for large-scale antenna array systems," *IEEE Trans. Signal Process.*, vol. 68, pp. 3529–3544, May 2020.
- [36] Y. Wang, Y. Wu, and Y. Shen, "Cooperative tracking by multi-agent systems using signals of opportunity," *IEEE Trans. Commun.*, vol. 68, no. 1, pp. 93–105, Jan. 2020.
- [37] *IEEE Standard for Local and Metropolitan Area Networks—Part 15.4: Low-Rate Wireless Personal Area Networks (LR-WPANs)*, IEEE Standard 802.15.4-2011 (Revision of IEEE Std 802.15.4-2006), Sep. 2011, pp. 1–314.
- [38] S. Wedge, "Predicting random jitter—Exploring the current simulation techniques for predicting the noise in oscillator, clock, and timing circuits," *IEEE Circuits Devices Mag.*, vol. 22, no. 6, pp. 31–38, Nov. 2006.
- [39] S. P. Chepuri, R. T. Rajan, G. Leus, and A.-J. van der Veen, "Joint clock synchronization and ranging: Asymmetrical time-stamping and passive listening," *IEEE Signal Process. Lett.*, vol. 20, no. 1, pp. 51–54, Jan. 2013.
- [40] J. Walker and A. Cantoni, "Modeling the effect of nonideal reference clocks on the jitter generated in timing transfer," *IEEE Trans. Commun.*, vol. 55, no. 1, pp. 44–47, Jan. 2007.
- [41] J. Walker and A. Cantoni, "Modeling of the synchronization process jitter spectrum with input jitter," *IEEE Trans. Commun.*, vol. 47, no. 2, pp. 316–324, Feb. 1999.
- [42] J. Walker and A. Cantoni, "Experimental evaluation of the jitter generated in timing transfer," *IEEE Trans. Commun.*, vol. 58, no. 12, pp. 3605–3612, Dec. 2010.
- [43] EPSON. (May 2016). *Crystal Oscillator Datasheet: SG2016/3225/5032/7050CAN*. [Online]. Available: https://support.epson.biz/td/api/doc_check.php?dl=app_SG2016CAN&lang=en
- [44] Y. Shen, H. Wymeersch, and M. Z. Win, "Fundamental limits of wideband localization—Part II: Cooperative networks," *IEEE Trans. Inf. Theory*, vol. 56, no. 10, pp. 4981–5000, Oct. 2010.
- [45] Y. Shen and M. Z. Win, "Fundamental limits of wideband localization—Part I: A general framework," *IEEE Trans. Inf. Theory*, vol. 56, no. 10, pp. 4956–4980, Oct. 2010.
- [46] D. Dardari, A. Conti, U. Ferner, A. Giorgetti, and M. Z. Win, "Ranging with ultrawide bandwidth signals in multipath environments," *Proc. IEEE*, vol. 97, no. 2, pp. 404–426, Feb. 2009.
- [47] S. Dwivedi, A. De Angelis, D. Zachariah, and P. Händel, "Joint ranging and clock parameter estimation by wireless round trip time measurements," *IEEE J. Sel. Areas Commun.*, vol. 33, no. 11, pp. 2379–2390, Nov. 2015.
- [48] I. Borg and P. Groenen, *Modern Multidimensional Scaling: Theory and Applications*. New York, NY, USA: Springer, 2005.
- [49] H. W. Wei, R. Peng, Q. Wan, Z. X. Chen, and S. F. Ye, "Multidimensional scaling analysis for passive moving target localization with TDOA and FDOA measurements," *IEEE Trans. Signal Process.*, vol. 58, no. 3, pp. 1677–1688, Mar. 2010.
- [50] C. Wang, J. Wang, Y. Shen, and X. Zhang, "Autonomous navigation of UAVs in large-scale complex environments: A deep reinforcement learning approach," *IEEE Trans. Veh. Technol.*, vol. 68, no. 3, pp. 2124–2136, Mar. 2019.
- [51] Y. Cai and Y. Shen, "An integrated localization and control framework for multi-agent formation," *IEEE Trans. Signal Process.*, vol. 67, no. 7, pp. 1941–1956, Apr. 2019.
- [52] Y. Liu, Y. Wang, J. Wang, and Y. Shen, "Distributed 3D relative localization of UAVs," *IEEE Trans. Veh. Technol.*, vol. 69, no. 10, pp. 11756–11770, Oct. 2020.
- [53] K. S. Arun, T. S. Huang, and S. D. Blostein, "Least-squares fitting of two 3-D point sets," *IEEE Trans. Pattern Anal. Mach. Intell.*, vol. PAMI-9, no. 5, pp. 698–700, Sep. 1987.



Zijian Zhang (Student Member, IEEE) received the B.E. degree in electronic engineering from Tsinghua University, Beijing, China, in 2020, where he is currently pursuing the Ph.D. degree in electronic engineering. His research interests include physical-layer algorithms for massive MIMO and reconfigurable intelligent surface (RIS). He received the National Scholarship in 2019 and the Excellent Thesis Award of Tsinghua University in 2020.



Hanying Zhao (Student Member, IEEE) received the B.E. degree (Hons.) in information engineering from Xidian University, Xi'an, China, in 2016. She is currently pursuing the Ph.D. degree in electronic engineering with Tsinghua University, Beijing, China.

Her research interests include statistical signal processing, optimization, and network localization.



Jian Wang (Senior Member, IEEE) received the Ph.D. degree in electronic engineering from Tsinghua University, Beijing, China, in 2006. In 2006, he joined as a faculty of Tsinghua University, where he is currently a Professor with the Department of Electronic Engineering. His research interests include application of statistical theories, optimization, machine learning to communication, networking, navigation, and resource allocation problems, in particular heterogeneous networks and intelligent collaborative systems.



Yuan Shen (Senior Member, IEEE) received the B.E. degree (Hons.) in electronic engineering from Tsinghua University, Beijing, China, in 2005, and the S.M. degree in electrical engineering and computer science and the Ph.D. degree from MIT, Cambridge, MA, USA, in 2008 and 2014, respectively.

He is currently an Associate Professor with the Department of Electronic Engineering, Tsinghua University. His research interests include network localization and navigation, inference techniques, resource allocation, and cooperative networks. He has served as the TPC Symposium Co-Chair for the IEEE ICC and IEEE GLOBECOM for several times. He was the Elected Chair of the IEEE ComSoc Radio Communications Committee from 2019 to 2020. He is an Editor of the IEEE TRANSACTIONS ON WIRELESS COMMUNICATIONS, IEEE WIRELESS COMMUNICATIONS LETTERS, and *China Communications*.